Stony Brook University

Genetic Regulation of Bone Morphology is highly Site-Specific within the Mouse Femur

A Thesis Presented

by

Paul Emilio Peña

to

The Graduate School

In Partial Fulfillment of the

Requirements

for the Degree of

Master of Science

in

Biomedical Engineering

Stony Brook University

December 2008

Stony Brook University

The Graduate School

Paul Emilio Peña

We, the thesis committee for the above candidate for the

Master of Science degree,
hereby recommend acceptance of this thesis.

Stefan Judex, Ph.D. – Thesis Advisor
Associate Professor, Department of Biomedical Engineering

Yi-Xian Qin, Ph.D. – Chairperson of Defense
Professor, Department of Biomedical Engineering

Kristian Carlson, Ph.D.
Assistant Professor, Department of Anatomy, NYCOM

This thesis is accepted by the Graduate School

Lawrence Martin
Dean of the Graduate School

Abstract of the Thesis

Genetic Regulation of Bone Morphology is highly Site-Specific within the Mouse Femur

by

Paul Emilio Peña

Master of Science

in

Biomedical Engineering

Stony Brook University

2008

Fractures are one of the most common bone injuries in the United States. Twenty billion dollars is spent annually to treat over a million people. Current methods of assessing fracture risk focus on measuring bone mineral density (BMD), which has been identified as a measurement that does not fully predict fracture risk. In addition, risk prediction depends on the skeletal site being measured; however, the number of existing skeletal sites has not been identified for a heterogeneous population. The objective of this study is to determine how specific is the regional morphology defined within an entire bone. We hypothesize that in a genetically heterogeneous population, regional morphologies within the entire femur are not correlated to each other. We conducted our study on a adult F2 heterogeneous population. We harvested their femurs and scanned six predefined regions with micro-computed tomography (μCT). The six regions consist of the head (H), neck (N), proximal metaphysis (PM), mid-diaphysis (MD), distal metaphysis (DM) and distal epiphysis (DE). Trabecular and cortical indices were measured and then correlated between the different regions. Trabecular bone proved to be genuinely site specific while cortical bone did not. Despite this result, trabecular bone was moderately correlated to cortical bone. Mouse weights and femora lengths had little to no influence in the correlations between the femoral regions. This study indicates that for future fracture risk diagnostic methods, site specificity would have to be considered because even within a location of the bone (proximal or distal) site specific morphology is still being defined.

Table of Contents

List of Symbols

μCT - Micro-Computed Tomography

ApoE - Apolipoprotein E

BALB - BALB/cByJ

BMD - Bone Mineral Density

BV - Bone Volume

BV/TV- Bone Volume Fraction

C3H - C3H/HeJ

Conn.D - Connectivity Density

Ct - Cortical

CT - Computed Tomography

Ct.Ar – Cortical Area

Ct.BV – Cortical Bone Volume

Ct.BV/TV – Cortical Bone Volume Fraction

Ct.Th – Cortical Thickness

Ct.TMD – Cortical Tissue Mineral Density

DE - Distal Epiphysis

DM – Distal Metaphysis

DXA - Dual X-ray Absorptiometry

ERα - Estrogen Receptor Alpha

H - Head

IL-6 - Interleukin 6

I_{max} – Maximum Moment of Inertia

I_{min} – Minimum Moment of Inertia

I_p – Polar Moment of Inertia

MD – Mid-Diaphysis

N - Neck

n - Sample Size

PM –Proximal Metaphysis

QCT - Quantitative Computed Tomography

ROI - Region Of Interest

SD – Standard Deviation

SMI – Structural Model Index

Tb - Trabecular

Tb.N -Trabecular Number

Tb.Th – Trabecular Thickness

Tb.TMD – Trabecular Tissue Mineral Density

TGFβ - Transforming growth factor beta

TMD – Tissue Mineral Density

VDR - Vitamin D Receptor

List of Figures

List of Tables

Chapter 1

Introduction

Overview

With fracture risk being a great health concern, considering site-specific morphology to predict bone strength may improve the quality of life for many patients. Currently, BMD is being used as a measure to predict fracture risk, however, it is not fully predictive and perhaps considering site-specificity may provide for a more accurate measurement of bone strength. Specificity can be depicted at the microarchitectural level of bone and in order to appreciate this concept understanding the factors that influence bone biology at this level is very important.

Bone Function and Biology

The skeleton functions primarily to provide structural support and a framework for the human body. Bone is capable of these functions primarily because of the tissue's balance in stiffness and elasticity. The stiffness property in bone permits it to support a load while its ductility permits it to minimize the load by absorbing its energy [1, 2]. This balance in properties allows bone to be light yet strong. For example, the hip can support eight times the weight of the human body [3].

Bone modeling and remodeling are the basic mechanisms that give bone the ability to maintain a balance in its tissue properties. These mechanisms effectively control the amount of mineral content in bone, where the more mineral is created in bone the stiffer the bone gets [4]. Once bone has developed an amount of mineral content for peak bone strength, it tries to maintain that amount through the mechanism of remodeling [1]. In maintaining the same amount of mineral content, remodeling changes the geometry and mineral distribution in bone optimizing the appropriate elastic and stiffness properties [5]. For example, near the shaft of the femoral neck the cortical shell is thick and elliptical; however, at the proximal end of the neck the cortical shell is more circular and has more trabecular bone. Both ends of the femoral neck have the same amount of bone content, suggesting the influence of a morphological adjustment in order to maintain peak bone strength [5]. Remodeling, however, is not always consistent. Once human bone has reached its adult form, adjustments to maintain peak bone strength become less successful through remodeling, and even less successful with age [1]. In addition, diseases (osteoporosis) and drugs (bisphosphonate) are known to impact remodeling and reduce peak bone strength [6].

The potential increase in fracture risks in the future has made assessing and studying the determinants of fracture risk very important. However, in order for us to appreciate the work that has been achieved in assessing and studying fracture risk, it is important to

first have a brief understanding of bone biology. When studying bone strength, it is important to understand that the overall mechanisms controlling bone strength are bone modeling and remodeling [Figure 1]. Bone modeling is defined as a process of laying down bone onto a bone surface that has never been previously resorb, where resorption would occur at a different surface from formation [2]. Bone remodeling is a process where bone resorption and formation occurs on the bone surface. Remodeling generally occurs for replacing dead or damaged tissue in addition to adapting to changes in loading and in response to nutritional and metabolic changes [7, 8]; these changes are induced in an effort to achieve and/or maintain peak bone strength. One example of remodeling is illustrated in the process of longitudinal growth in the long bone, when the metaphyseal region of the bone grows it forms into a shaft-like shape resembling the diaphysis. The change in shape occurs through the periosteal and endosteal surfaces [9-11].

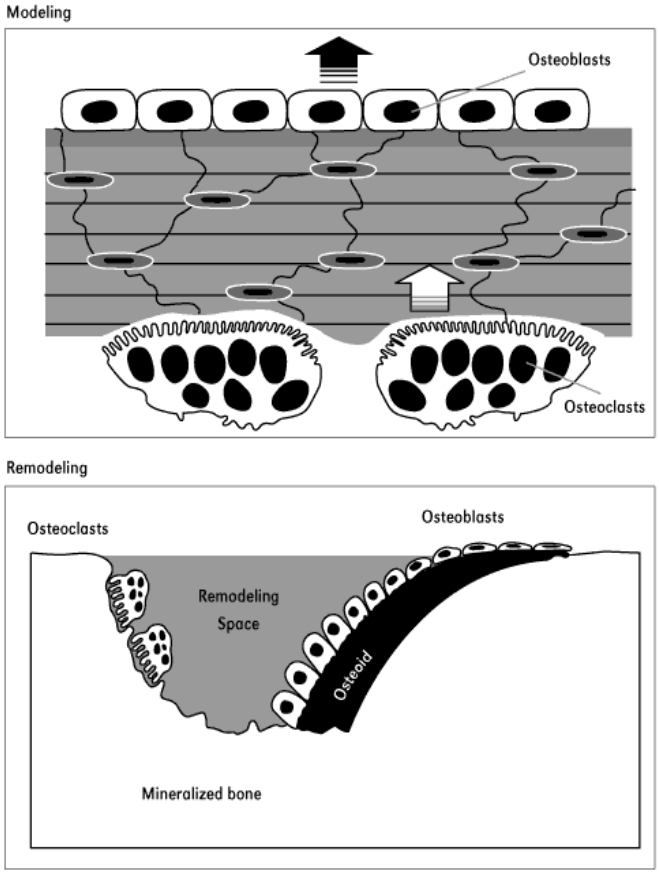

Figure 1. An illustration of bone modeling and remodeling. In modeling, osteoclasts and osteoblasts are not linked and occur at different surfaces. In remodeling, the osteoblasts are coupled with osteoclasts and provide bone formation after resorption in the region [12].

The general structure of bone consists of an inner and outer compartment [Figure 2]. In long bones, the inner compartment consists of trabecular (spongy) bone and the endosteal surface (except the diaphysis). Trabeculae are shaped like rods or plates and are arranged in a lattice-like structure with many of the struts parallel to the direction of stress [13]. The trabecular compartment helps transfer a load that is applied to a bone.

The transferred loads can be redistributed after appropriate remodeling has taken place. The endosteal surface lines the inner cavity of the long bone, creating a layer that surrounds the trabecular surface. The outer compartment consists of the cortical shell and periosteal surface. The cortical shell is mainly, however, not entirely cylindrical in shape and it has very little porosity. The outer compartment usually must withstand bending and torsional forces. The periosteum is the outer layer of the outer compartment, and like the endosteal surface. It is known to be the site where most remodeling occurs.

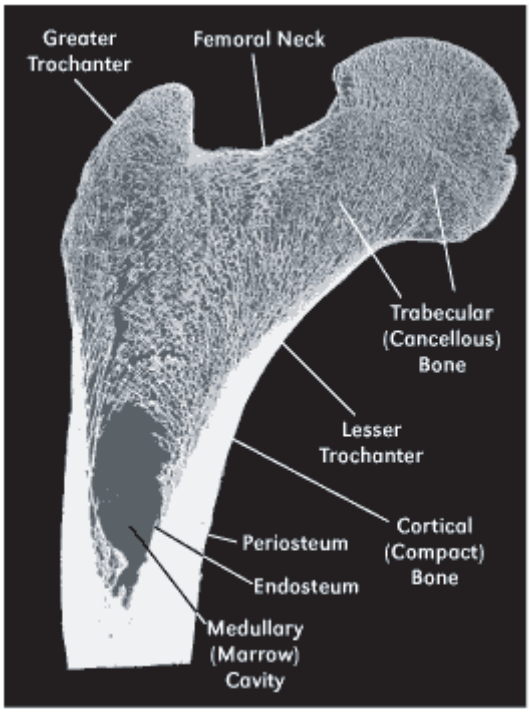

Figure 2. Image of femoral head illustrating the inner and outer compartment of bone [14]. Note lesser trochanter not visible in image.

Both the organic and inorganic components of bone are involved in remodeling. The extracellular matrix of bone is 70% inorganic, 25% organic, and 5% water. The inorganic portion is mainly hydroxyapatite (which includes calcium and phosphate ions). The cells that make up the bone and its matrix are mainly osteoblasts, osteoclasts, and osteocytes [2]. Osteoblasts are cells that lay down extracellular matrix and they communicate with their environment by anchoring to the skeletal matrix or to other cells. Due to it's their anchoring abilities, osteoblasts are very well connected in bone and this gives osteoblasts the ability to sense metabolic and mechanical demands to direct bone formation [15, 16]. Osteoclasts are cells that resorb mineralized bone (the calcium and phosphate component) with vesicles. When osteoclasts are activated, they are capable of absorbing 200,000 μm^3 of mineral per day, an amount that is produced by 7-10 generations of osteoblasts that have a 15-20 day lifespan [17]. Osteocytes are the most abundant of bone cells, and they function primarily as a mechanosensory cells that determine bone structure [18]. As mechanosensory cells, it is believed that osteocytes are

the cells that maintain mineral homeostasis in bone; specifically, as releasers of hormones and factors that signal for osteoclastic resorption [19].

Impact of Fractures

According to the World Health Organization, osteoporosis is defined as a disease that causes a reduction in bone mass and a structural deterioration of bone tissue, leading to bone fragility and increased susceptibility to fractures [20]. The increase in skeletal fragility is caused by an excessive resorption of bone with an insufficient amount of bone formation, which results in an inadequate balance of stiffness and elasticity. There are approximately 1.3 million individuals that suffer from osteoporotic fractures; osteoporotic fractures account for 70% of all fractures in the United States, of which the most common are hip, vertebra, and distal forearm (wrist) fractures [21]. Other sites of fracture that are not as common include the proximal humerus, pelvis, proximal tibia and distal femur [22]. Osteoporosis is linked with a 10-20% reduction in patient survival following hip fracture [23]. Morbidity increases approximately 7-8% after patients develop an osteoporotic hip, or spine and wrist fractures, which often result in patient placement in a nursing home [24]. The overall cost of osteoporotic fractures is also an enormous burden since $20 billion is spent annually in the United States, and hip fractures account for a third of this total [25]. It is also projected that the number of people in the world that are affected by fractures will increase in the future. It is estimated that among men and women over the age of 65 numbers of people affected by osteoporosis will climb from 323 million to 1.5 billion by the year of 2050 [26].

There have been several factors identified as predictors of skeletal fragility: history of a previous fracture, bone mineral density (BMD), bone turnover (remodeling), microarchitecture, mineralization, microdamage, collagen crosslinking, and mineral crystal structure [27]. The use of bone turnover, history of fracture and BMD as predictors of fracture has been established in a research setting. In the clinical setting, BMD was once the gold standard for predicting fracture [27]. It was believed that higher BMD would increase bone strength and a lower amount would reduce strength. However, BMD alone cannot predict fracture risk. It has been shown that when BMD levels rise from 9% to 13%, the assessment for fracture risk does not change [27]. This indicates that magnitude of BMD and bone strength can be independent phenomena, and thus proves that other factors warrant consideration in order to provide a complete assessment of fracture risk [28, 29]. The image modality commonly used by clinicians to assess BMD is dual x-ray absorptiometry (DXA), however, studies have shown that this modality is limited to assessing areas rather than volume [30]. Volumetric information is important because it is more indicative of potential changes in mass, geometry and overall morphology of a bone.

Of the factors identified as predictors for skeletal fragility none have been implanted into a potential diagnostic tool (except BMD) except for microarchitecture. The volumetric information for bone consists of a characterization of the bone's microstructure. And this information can be attained with a high-resolution computed tomography (CT) scanner such as the peripheral QCT. While these scanners have not been established as diagnostic tools yet because of their high x-ray exposure, advances in

scanner technology are leading towards potential cortical and trabecular tissue information that will permit closely measuring skeletal fragility [30]. While the improvement of technology will come with time, current research has focused on extracting the most relevant microarchitectural information using micro CT scanners.

Research on the genetic regulation of osteoporosis indicates that there are many genes involved in controlling or influencing osteoporosis. In a twin study and a family fracture study, genetics accounted for 50-80% of the variability in bone mass [31-34]. In post-menopausal women, heredity accounted for 25-54% of the variation in wrist fracture incidence; the women showed variability in percentage due to age (as age increased genetics explained less variation in fracture incidence) and heritability was largely, but not entirely, independent of BMD suggesting genetic control over other fracture factors, such as bone turnover and geometry [35, 36]. Risk factors for osteoporotic fractures, such as quantitative ultrasound properties, geometry and bone turnover have been shown to have strong heritable components [20, 37, 38]. One of the gene candidates believed to influence osteoporosis during bone growth is VDR; other candidates associated with osteoporosis control include ERα, ApoE, IL-6, TGFβ and MTHFR [39]. However, these genes are also known to influence other conditions. Thus, it is important to elucidate the roles of genes in osteoporosis. The VDR gene is associated with diabetes, hyperthyroidism and multiple sclerosis, while the ApoE gene has been implicated in ischemia and Alzheimer's disease.

A better diagnostic tool for predicting fracture is possible when using high resolution CT scanners to assess bone morphology. A microarchitectural analysis reveals information on bone quantity and quality. In osteoporotic bone, trabeculae are reduced in numbers, connections, and thickness [40]. Apparently these changes in trabecular structure result in osteoporotic bone having an inability to transfer loads properly [40, 41]. Men exhibiting a vertebral fracture have lower bone interconnectivity and trabecular number compared to men without a vertebral fracture [42]. In a separate study of hip fracture patients, overall geometry changed in order to reduce stress; the diameter of the bone increased more in fracture patients than non-fracture patients [43]. Likewise, women who suffer from femoral neck fractures tended to have wider femoral necks and femoral neck shafts [36, 44, 45]. Most of these studies observed bone morphology as a whole; however, site-specific regions exist in bones. In future assessments of bone fracture risks, the strategy of studying morphology should include site-specificity.

Site specificity varies significantly with genetic background, yet there no indication if the degree of specificity is greater for one genetic background over another, and visa versa. In a study comparing three genetically distinct mice, it was shown that no particular expression for site specificity could be linked to a specific type of genetic background [46]. The study was based on correlations with regions in the distal end of the femur; a similar study looking at an entire bone within a heterogeneous population may provide more information on any trends of dominance with genetic background. In a similar study, it was shown that depending on the genetic background, the site specific response to bone disuse varied significantly [47]. Some responses include uniform bone loss among specific sites of a bone, a compensatory effect when bone is lost in one site but gained in another or completely different degrees of loss at different sites without compensation at other sites. Since the study focused on a limited amount of mouse

strains and site specific regions, a study on an entire bone and form a population of genetically distinct mice may be more indicative of potential responses for particular genetic backgrounds. Subsequent studies have focused on different aspects of site specificity such as: the uniform effect of drugs on site-specific regions; varied associations of single-nucleotide polymorphisms with different bone sites; differences of skeletal compartments (trabecular and cortical) between and among bone sites; non-uniform site specific increases in bone quantity after loading; and different genetic determinants for skeletal phenotypes within bone to the degree of different extents of genetic control for the two bone compartments [48-55].

Hypothesis and Specific Aim

It has thus become imperative to revisit the characterization of site-specificity in bone morphology. Previous analysis studied site-specificity on specific populations and skeletal sites. However, an analysis extended to an entire population and an entire bone will show how site-specificity in the grander scale. In addition, any trends that may exist in a genetically heterogeneous pool may be discovered since variability in bone mass and morphology are controlled by genetic factors [31-34]. Given microarchitecture is a key factor to fracture risk, understanding site-specificity in a bone's morphology will provide more accurate information on the relationship between genes and bone phenotype. Ultimately, developing an accurate and more informative imaging modality for patients could be achieved. Here, it is hypothesized that within a genetically heterogeneous population, regional morphologies within an entire bone are not correlated. If this can be demonstrated as true, it may suggest that site-specific morphology within an entire bone may be modulated by different combinations of genes. The specific aim of the research is to characterize site-specificity in bone microarchitecture by defining the level of site-specificity that exists among regions of the different bone tissues (i.e., trabecular and cortical).

Chapter 2

Materials and Methods

Heterogeneous Population

Previous studies have shown that using mice can serve as a proof of principle for studying characteristics of the human genotype and phenotype [46, 47, 56]. This study focuses on characterizing trabecular and cortical morphology in mice with micro-computed tomography and testing for correlations in these measures across different morphological regions of a bone. Criteria for choosing the mouse strains, BALB and C3H, were based on their distinction in BMD, which is a major indicator of bone strength (BALB having relatively lower BMD than C3H). Creating a heterogeneous population of mice by crossing these strains resulted in a distribution of morphologies that incorporated all possible combinations of the parental mice.
Male C3H/HeJ [C3H] and female BALB/cByJ [BALB] mice (Jackson Laboratory, Bar Harbor, ME) were raised until four months of age, after which the two strains were crossbred to create a first generation (F1) population. Subsequently, the F1 population was inbred into a second generation (F2) population of which 622 male mice were assigned to this study. Prior to sacrifice (at four months of age), the weight of the mice was approximately 40±5g. Femora were harvested from male mice, preserved in 70% ethanol (4°C), and scanned to conduct a morphological evaluation using a micro-computed tomography scanner (μCT40, Scanco Medical).

Experimental Design

Prior to scanning, samples were cleaned of all soft tissue, labeled for identification after scanning, and lengths measured with digital calipers. At least four bones were placed into a holder for simultaneous scanning. MicroCT scans were performed on the femur at a resolution of 12μm [46] (μCT40, Scanco Medical). Six regions of interest (ROIs) were investigated: one scan included the head, neck and proximal metaphysis ROIs; another scan included only the mid-diaphysis ROI, and a third scan included the distal metaphysis and distal epiphysis ROIs. After scanning, all ROIs were evaluated with algorithms that retrieved cortical and trabecular information [57]. Statistical tests were performed on morphometric and density information for both cortical and trabecular bone regions (SPSS Windows 15.0).

Terms and Measures

In this study, femora were divided into three morphological regions: proximal, middle and distal regions. The first region can be partitioned into three sub regions: the head, neck and proximal metaphysis [Figure 3]. The proximal end of the bone begins with the

femoral head (spherical), which predominantly consists of trabecular bone, and which is geometrically distinct from the neck region (cylindrical) that is comprised of both trabecular and cortical bone. The neck connects to the proximal metaphysis, which consists of both trabecular and cortical bone, with a similar geometry to the neck region, yet with a greater diameter in terms of trabecular bone. Distal to the proximal metaphysis, trabecular bone dissipates until only the cortical shell remains in the diaphysis. The diaphyseal region is the largest of all the regions in the femur. Only a portion of it was scanned in order to reduce scanning and evaluation time; this portion was focused on a landmark closest to the center of the diaphysis. The landmark was the most circular shell nearest to the center of the diaphyseal regions. Towards the distal end of the diaphysis, trabecular bone is considered in the analysis again. At the distal end, the distal metaphysis and distal epiphysis, both with trabecular and cortical bone but different geometry, were analyzed. The distal metaphysis was the longer of the defined regions in this study. The distal metaphysis ROI begins at 190 slices proximal to the condyles and ends 50 slices at the femoral condyles, while distal to the femoral condyles is the distal epiphysis ROI.

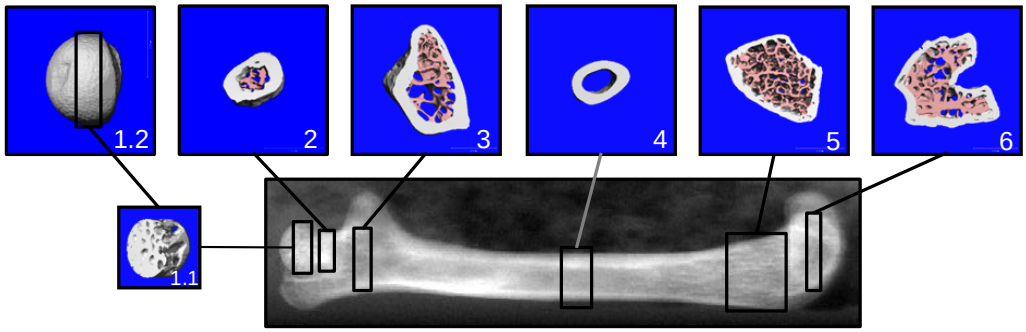

Figure 3: Renderings generated from the algorithm for the ROI in the femur. Figure 1.1 illustrates trabecular bone in the femoral head (Figure 1.2). This figure also shows the trabecular containing regions including the head (2), neck (3), distal metaphysis (5) and the distal epiphysis (6).The lone cortical shell is illustrated in the diaphysial region (4).

With the exception of the mid-diaphysis, femoral ROIs were chosen to include the maximum amount of trabecular bone and were evaluated with an automated algorithm that detects and separates trabecular and cortical bone. All images from the scans were reconstructed with a three-dimensional Gaussian filter for noise reduction and segmented in order to differentiate bone and non-bone using a global threshold. The ROIs for head (H) and neck (N) evaluations were defined by the algorithm as 480µm and 384µm in the z-axis, respectively. For the proximal metaphysis (PM), the ROI (456µm) was positioned according to a standard proximal metaphysis landmark: the location where the neck region fused with the greater trochanter, and the shape of the bone became consistently circular in cross-sectional geometry. Similarly, the mid-diaphysis (MD) ROI (756µm) began at the point closest to the center of the bone. First approximately 100 slices that revolve equally around the center of the bone is targeted. Within this region the most circular portion within this range selected to be the region where the slices were going to be analyzed between different bones. For the distal metaphysis (DM), the ROI (1500µm) begins 2316µm proximal to the distal metaphysis landmark, which is defined as the

region where fusion of the growth plate first appears at the distal end of the femur. The distal epiphysis (DE) ROI (360µm) begins at the landmark on the cross-section where the condyles disappear.

Data Validation

Using an automated algorithm, several morphological parameters were evaluated from trabecular and cortical bone in all of the scanned regions [57]. In order to validate proper derivation of the morphological parameters, the algorithm produces a 3D rendering of the evaluated ROI [Figure 4]. From 3D renderings, proper separation of trabecular and cortical bone at the specified ROI can be evaluated. In addition, magnitudes of results are reviewed relative to expected magnitudes at each ROI reported in previous studies to ensure proper calculations [58]. For trabecular bone, parameters of interest include: bone volume (BV), bone volume fraction (BV/TV), connectivity density (Conn.D), trabecular number (Tb.N), trabecular thickness (Tb.Th), tissue mineralized density of trabecular bone (Tb.TMD), and structure model index (SMI). For cortical bone parameters include cortical area (Ct.Ar), cortical bone volume (Ct.BV) cortical bone volume fraction (Ct.BV/TV), cortical thickness (Ct.Th), tissue mineralized density of cortical bone (Ct.TMD) and maximum, minimum and polar moments of inertia (I_{max}, I_{min}, I_p, respectively).

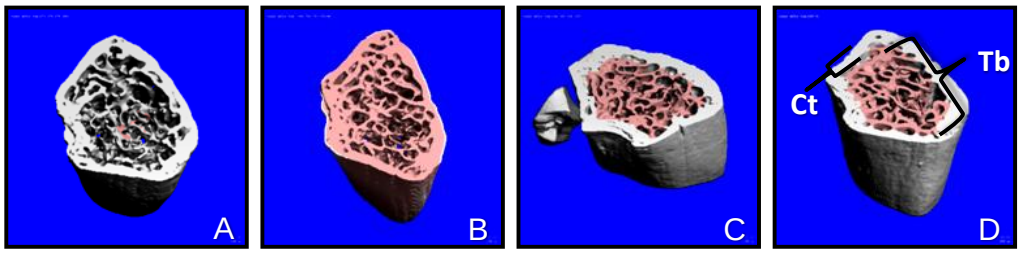

Figure 4. A 3D rendering of the ROI in the distal metaphysis, with trabecular (pink) and cortical (white) bone separation. Figure 4A depicts the lack of a separation of cortical shell from trabecular bone. Figure 4B depicts lack of separation of the trabecular bone from the cortical shell. Figure 4C depicts the inclusion of a fragment within the evaluation of the bone. Figure 4D is a depiction of the separation chosen to define the distal metaphyseal region. Ct = Cortical bone and Tb=Trabecular bone.

Statistics

Descriptive statistics (i.e., mean ± standard deviation) were compiled for the heterogeneous population relative to the parental mice. Trabecular and cortical bone values equivalent to the parental mean values are reported in a similar study [58]. These parental mice were male and 4 months of age and represented the control of a disuse study. Shapiro-Wilk normality tests (SPSS Windows 15.0) were used to assess distributions of trabecular and cortical data. Trabecular ancd cortical bone in different femoral regions was investigated using Pearson correlations. Partial Correlations were run using mouse weight and femora length as controlled values. Linear regressions were performed between significantly correlated regions to specify the degree of a correlated

relationship. All regressions were considered statistically significant when the associated p-value is less than 0.05.

Chapter 3

Results

Using the 3D rendering of the evaluated region of interest (ROI), we were able to verify that trabecular and cortical data were evaluated correctly. The total number of evaluated samples for each ROI was: n=296 for distal epiphysis, n=432 for distal metaphysis, n=360 for mid-diaphysis, n=436 for proximal metaphysis, and n=244 for head and neck regions. Note that the parental means that will be examined in the results come from a very similar study of the same lab group.

Distribution of Bone Indices and Properties from the Distal Metaphysis

Most of the indices and properties of the trabecular and cortical bone were normally distributed. Those that were not can be found in each trabecular and cortical regions, however, for each region the non-normally distributed indices and properties differed. Using the Shapiro-Wilk test on SPSS 15.0 for windows, it was found that in the distal metaphysis Tb.Th and Tb.Sp were not normally distributed values ($p < 0.05$). Both Tb.Th and Tb.Sp were slightly positively skewed and have normal curve peaks [Table 1]. In addition, all index and property distributions were superimposed with arrows of parental mean values to compare how each value existed relative to their parental mean values [Figure 5]. In the distal metaphysis, the mean values for BV/TV and Tb.Th were located toward the opposite ends of our offspring distribution. Specifically, the mean values of BV/TV and Tb.Th from the C3H mice were within 1SD below the grand means of the offspring distribution. The same mean values in the BALB mice were approximately 2 SD below the grand mean of our offspring distributions. In contrast, mean values for Tb.N, Tb.Sp, and Conn.D of C3H and BALB were very close to one another within their relatively wider offspring distribution. Another result unique to the distal metaphysis trabecular bone was that it contained the greatest mean value for BV and SMI and the lowest mean value for Tb.N [Appendix 1].

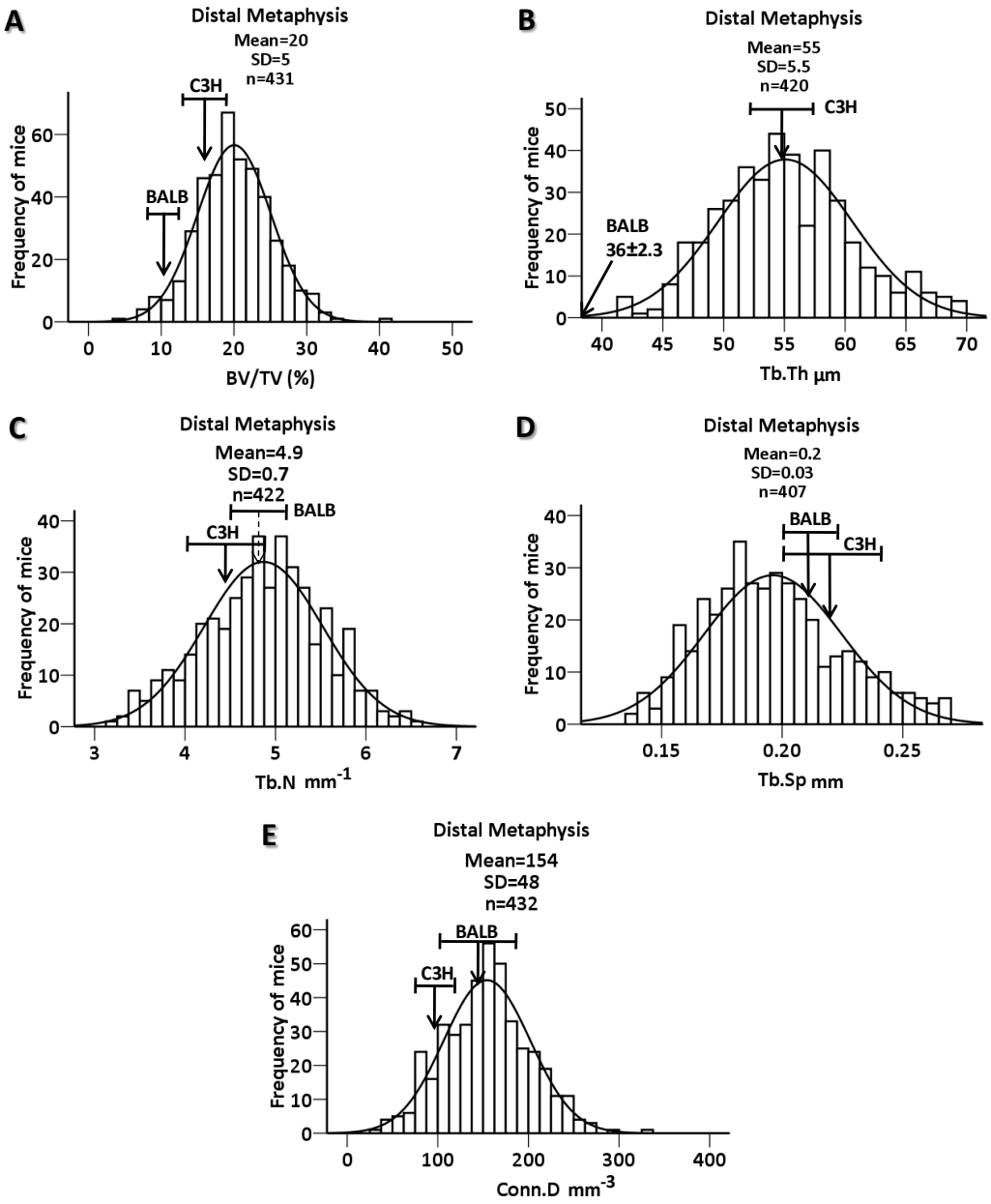

Figure 5. Offspring distribution of index values from the distal metaphyseal with parental means values in the form of arrows superimposed on the distribution. These values include (A) bone volume fraction, (B) trabecular thickness, (C) trabecular number, (D) trabecular spacing and (E) connectivity density. BV/TV and Tb.Th parental mean values are located on opposite ends of the offspring distributions and Tb.Th, Tb.N and Conn.D were not.

Table 1. Mean, SD, Shapiro-Wilk significance, skewness and kurtosis values of trabecular bone in the distal metaphysis region. Tb.Th and Tb.Sp are non-normally distributed in the heterogeneous population as tested by Shapiro-Wilk, where p was less than 0.05.

Descriptive Statistics of Trabecular Bone in the Distal Metaphysis

	N	Mean	SD	Shapiro-Wilk	Skewness		Kurtosis	
	Statistic	Statistic	Statistic	Sig.	Statistic	Std. Error	Statistic	Std. Error
BV (mm^3)	432	0.52	0.15	0.38	0.144	0.117	-0.194	0.234
BV/TV	431	20	5	0.52	0.117	0.118	0.444	0.235
Conn.D (mm^{-3})	432	154	48	0.38	0.145	0.117	0.086	0.234
SMI	430	1.4	0.42	0.53	-0.046	0.118	-0.21	0.235
Tb.N (mm^{-1})	422	4.9	0.66	0.19	-0.123	0.119	-0.317	0.237
Tb.Th (μm)	420	55	5.5	0.013	0.251	0.119	-0.115	0.238
Tb.Sp (mm)	407	0.2	0.03	0	0.432	0.121	-0.325	0.241
Tb.TMD ($g*mm^{-3}$)	439	236	52	0.09	-0.151	0.117	0.519	0.233

Table 2. Mean, SD, Shapiro-Wilk significance, skewness and kurtosis values of cortical bone in the distal metaphysis region. Ct.BV/TV and I_{min} are non-normally distributed as tested by the Shapiro-Wilk test.

Descriptive Statistics of Cortical Bone in the Distal Metaphysis

	N	Mean	SD	Shapiro-Wilk	Skewness		Kurtosis	
	Statistic	Statistic	Statistic	Sig.	Statistic	Std. Error	Statistic	Std. Error
Ct.BV (mm^3)	429	1.4	0.14	1	0.016	0.118	0.16	0.235
Ct.BV/TV (%)	424	79	3	0	1.03	0.119	0.46	0.237
Ct.Th (μm)	424	156	14	0.12	0.202	0.119	-0.126	0.237
I_p (mm^4)	430	0.7	0.13	0.07	0.273	0.118	0.203	0.235
I_{max} (mm^4)	430	0.49	0.09	0.17	0.241	0.118	0.253	0.235
I_{min} (mm^4)	427	0.21	0.04	0.01	0.181	0.118	-0.508	0.236
Ct.Ar (mm^2)	429	0.96	0.1	1	0.016	0.118	0.16	0.235
Ct.TMD ($g*mm^{-3}$)	438	873	31	0.47	-0.16	0.12	0.05	0.23

From the cortical bone of the distal metaphyseal region, only Ct.BV/TV and I_{min} departed from normality (Shapiro-Wilk p value < 0.05). Ct.BV/TV was positively skewed and slightly leptokurtic, while I_{min} was not significantly skewed and exhibits a lower peak than normal Gaussian (platykurtic) [Table 2]. Parental mean values for Ct.Ar, I_p, I_{max} and I_{min} were located toward opposite ends of the offspring distribution, where the mean of C3H mice was 1 SD above the grand mean for all offspring distributions, while BALB mice had means mainly greater but within 1 SD of grand means for all offspring distributions of these indices [Figure 6]. Relative to all other regions, the distal metaphysis had the greatest mean for Ct.BV [Appendix 2].

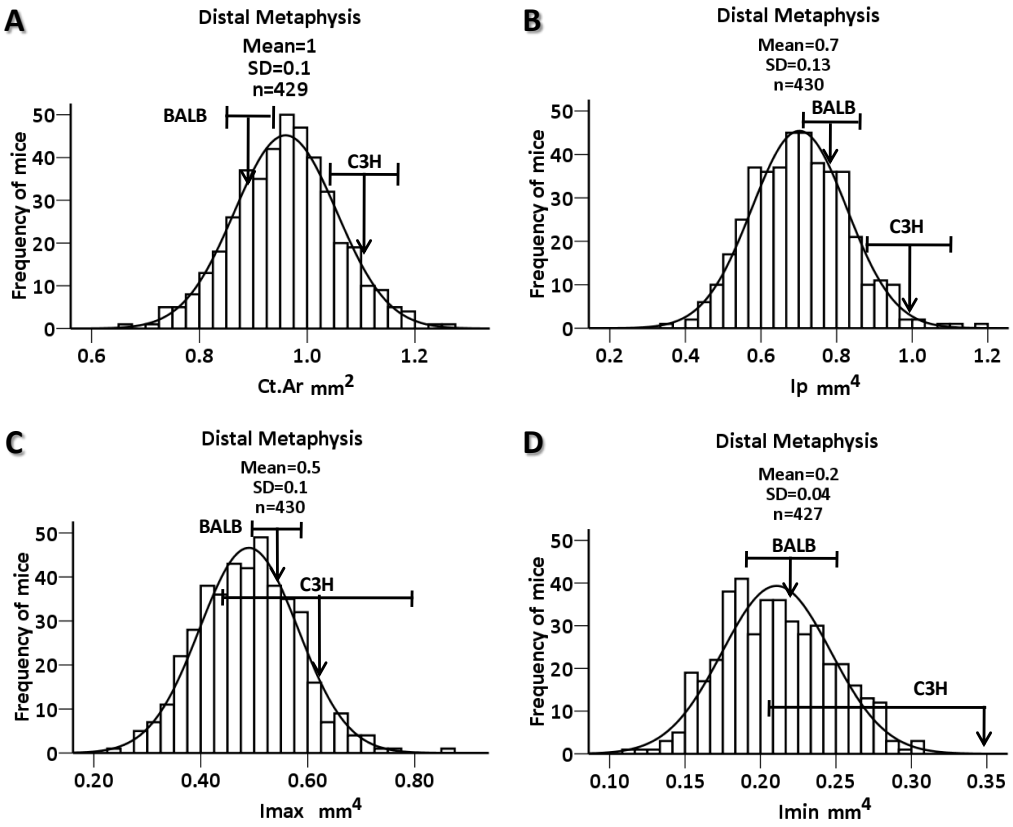

Figure 6. Offspring distribution of index and property values from the distal metaphyseal with parental means values in the form of arrows superimposed on the distribution. These values include (A) Ct.Ar, (B) Tb.Th (C) Tb.N, and (D) Tb.Sp. Ct.Ar and all moments of inertia parental mean values were at opposite end of offspring distribution

Distribution of Bone Indices and Properties from the Distal Epiphysis

Within the distal epiphysis, only indices Tb.TMD, Conn.D and Tb.N departed significantly from normal distributions of the heterogeneous population (Shapiro Wilk $p < 0.05$). Conn.D was slightly positively skewed and with a significantly normal peak, while Tb.N was positively skewed and with a significantly normal peak, and Tb.TMD was positively skewed and peaks leptokurtically [Table 3]. Mean values of Tb.Th, Tb.N, Tb.Sp, and Conn.D from the parental strain were located toward the opposite ends of the offspring distribution. However, mean values of BV/TV for the C3H and BALB mice were located below the population mean, but within 1 SD of the population mean [Figure 7]. Mean values for both parental groups were not significantly different from one another (confirmed with an ANOVA). Relative to all other regions, the distal epiphysis had the greatest mean for BV/TV and the lowest mean for SMI [Appendix 1].

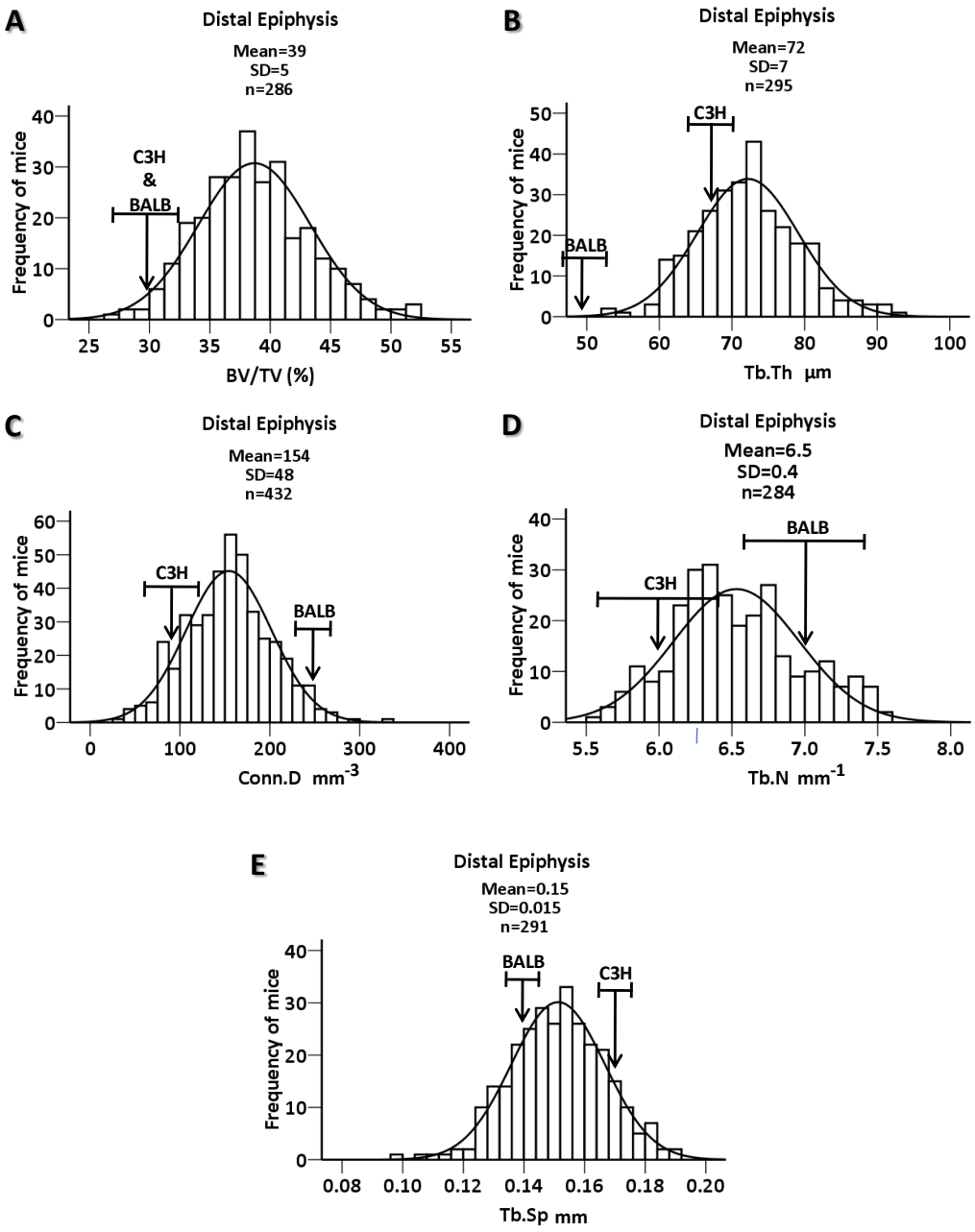

Figure 7. Offspring distribution of index values from the distal epiphysis with parental means values in the form of arrows superimposed on the distribution. These values include (A) BV/TV, (B) Tb.Th (C) Conn.D, (D) Tb.N and (E) Tb.Sp. Tb.Th, Tb.N, Tb.Sp and Conn.D parental mean values were at the opposite end of offspring distribution. Both parental means for BV/TV, however, were within 1 SD of the grand mean in the offspring distribution.

Table 3. Mean, SD, Shapiro-Wilk significance, skewness and kurtosis values of trabecular bone in the distal epiphysis region. Conn.D, Tb.N and Tb.TMD were non-normally distributed as tested by the Shapiro-Wilk test.

Descriptive Statistics of Trabecular Bone in the Distal Epiphysis

	N	Mean	SD	Shapiro-Wilk	Skewness		Kurtosis	
	Statistic	Statistic	Statistic	Sig.	Statistic	Std. Error	Statistic	Std. Error
BV (mm^3)	291	0.330	0.060	0.79	0.071	0.143	0.332	0.285
BV/TV (%)	286	39	4.6	0.06	0.342	0.144	0.017	0.287
Conn.D (mm^{-3})	290	137	32	0	0.377	0.143	-0.34	0.285
SMI	295	-0.37	0.42	0.59	-0.189	0.142	0.153	0.283
Tb.N (mm^{-1})	284	6.5	0.43	0.001	0.31	0.145	-0.409	0.288
Tb.Th (μm)	295	72	6.9	0.32	0.221	0.142	0.071	0.283
Tb.Sp (mm)	291	0.15	0.02	0.67	-0.122	0.143	0.109	0.285
Tb.TMD ($g*mm^{-3}$)	296	398	50	0.007	0.345	0.142	1	0.282

Table 4. Mean, SD, Shapiro-Wilk significance, skewness and kurtosis values of cortical bone in the distal epiphysis region. Ct.BV/TV and Ct.Th were non-normally distributed as tested y the Shapiro-Wilk test.

Descriptive Statistics of Cortical Bone in the Distal Epiphysis

	N	Mean	SD	Shapiro-Wilk	Skewness		Kurtosis	
	Statistic	Statistic	Statistic	Sig.	Statistic	Std. Error	Statistic	Std. Error
Ct.BV (mm^3)	293	0.48	0.048	0.07	0.315	0.142	0.098	0.284
Ct.BV/TV (%)	296	75	6.5	0	0.224	0.142	-1.108	0.282
Ct.Th (μm)	296	109	14	0	0.343	0.142	-0.624	0.282
I_p (mm^4)	291	1.03	0.17	0.77	-0.066	0.143	-0.160	0.285
I_{max} (mm^4)	292	0.57	0.09	0.8	-0.113	0.143	-0.149	0.284
I_{min} (mm^4)	292	0.46	0.09	0.37	-0.091	0.143	-0.009	0.284
Ct.Ar (mm^2)	292	1.3	0.13	0.21	0.215	0.143	-0.193	0.284
Ct.TMD ($g*mm^{-3}$)	287	741	35	0.79	-0.05	0.141	0.136	0.282

All cortical variables from the distal epiphyseal region, except Ct.Th (positively skewed, platykurtic, and almost bimodal) and Ct.BV/TV (positively skewed, platykurtic, and almost bimodal) did not depart significantly from normal distributions [Table 4]. Relative to all other regions, the distal epiphysis had the greatest mean for I_p and the lowest mean for Ct.Th and Ct.TMD [Appendix 2].

Distribution of Bone Indices and Properties from the Mid-Diaphysis

In the mid-diaphysis, only Ct.BV/TV and Ct.TMD departed from normal distribution within all cortical variables and properties. Ct.BV/TV was not significantly skewed and had a normally curved peak, however, Ct.TMD was positively skewed and had a leptokurtic peak [Table 5]. Mean values of the parental strains for Ct.Ar, I_p, I_{max}, and I_{min} were located toward the opposite ends of the offspring distribution, where the mean of C3H mice was closer to the higher values for these indices and the mean of BALB mice was towards the lower end [Figure 8]. Relative to all other regions, the diaphysis had the greatest mean for Ct.BV/TV, Ct.TMD and Ct.Th [Appendix 2].

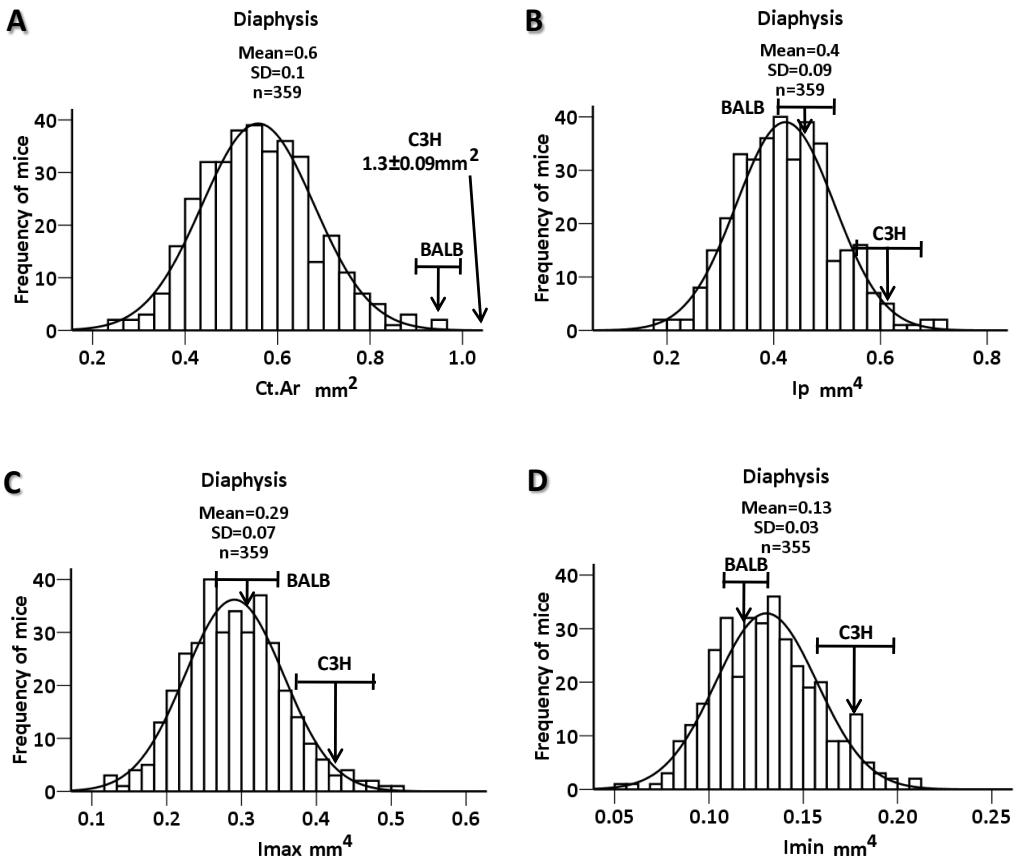

Figure 8. Offspring distribution of index values from the mid-diaphysis with parental means values in the form of arrows superimposed on the distribution. These values include (A) Ct.Ar, (B) I_p (C) I_{max} and (D) I_{min}, and all were located toward opposite ends of the offspring distribution.

Table 5. Mean, SD, Shapiro-Wilk significance, skewness and kurtosis values of cortical bone in the mid-diaphysis region. Ct.BV/TV and Ct.TMD were non-normally distributed as tested y the Shapiro-Wilk test.

Descriptive Statistics of Cortical Bone in the Mid-Diaphysis

	N	Mean	SD	Shapiro-Wilk	Skewness		Kurtosis	
	Statistic	Statistic	Statistic	Sig.	Statistic	Std. Error	Statistic	Std. Error
Ct.BV (mm^3)	360	0.76	0.09	0.68	-0.027	0.129	0.205	0.256
Ct.BV/TV (%)	348	99	0.1	0.039	-0.242	0.131	-0.281	0.261
Ct.Th (μm)	360	312	33	0.38	0.179	0.129	0.146	0.256
I_p (mm^4)	359	0.42	0.09	0.1	0.305	0.129	0.196	0.257
I_{max} (mm^4)	359	0.29	0.07	0.12	0.283	0.129	0.159	0.257
I_{min} (mm^4)	355	0.13	0.027	0.07	0.240	0.129	-0.195	0.258
Ct.Ar (mm^2)	359	0.56	0.12	0.1	0.305	0.129	0.196	0.257
Ct.TMD ($g*mm^{-3}$)	467	1208	23	0.01	0.249	0.113	0.71	0.225

Distribution of Bone Indices and Properties from the Proximal Metaphysis

In the proximal metaphysis, Tb.N and Tb.TMD were the only trabecular indices that were non-normally distributed (Shapiro-Wilk $p<0.05$). The Tb.N distribution was not significantly skewed and slightly but not significantly platykurtic; Tb.TMD is negatively skewed and slightly but not significantly leptokurtic [Table 6]. All cortical variables were normally distributed within the proximal metaphyseal [Table 7]. Relative to all other regions, the proximal metaphysis had the greatest mean for Tb.Sp and I_{max}, and the lowest for Tb.TMD [Appendix 1].

Table 6. Mean, SD, Shapiro-Wilk significance, skewness and kurtosis values of trabecular bone in the proximal metaphyseal region. Tb.N was non-normally distributed as tested y the Shapiro-Wilk test.

Descriptive Statistics of Trabecular Bone in the Proximal Metaphysis

	N	Mean	SD	Shapiro-Wilk	Skewness		Kurtosis	
	Statistic	Statistic	Statistic	Sig.	Statistic	Error	Statistic	Error
BV (mm^3)	436	0.15	0.03	0.1	-0.1	0.117	0.557	0.233
BV/TV (%)	435	17	3.3	0.847	0.043	0.117	-0.244	0.234
Conn.D (mm^{-3})	436	98	23	0.955	0.091	0.117	-0.077	0.233
SMI	436	0.64	0.36	0.053	0.269	0.117	0.192	0.233
Tb.N (mm^{-1})	430	5.1	0.43	0.03	0.156	0.118	-0.445	0.235
Tb.Th (μm)	436	59	4.5	0.274	0.048	0.117	0.602	0.233
Tb.Sp (mm)	435	0.21	0.02	0.18	0.166	0.117	0.236	0.234
Tb.TMD ($g*mm^{-3}$)	435	207	37	0.001	-0.46	0.117	0.449	0.234

Table 7. Mean, SD, Shapiro-Wilk significance, skewness and kurtosis values of cortical bone in the proximal metaphyseal region. All indices and properties were normally distributed as tested y the Shapiro-Wilk test.

Descriptive Statistics of Cortical Bone in the Proximal Metaphysis

	N	Mean	SD	Shapiro-Wilk	Skewness		Kurtosis	
	Statistic	Statistic	Statistic	Sig.	Statistic	Std. Error	Statistic	Std. Error
Ct.BV (mm^3)	435	0.66	0.059	0.197	0.218	0.117	-0.081	0.234
Ct.BV/TV (%)	435	89	3	0	0.443	0.117	-1.177	0.234
Ct.Th (μm)	432	213	16.7	0.021	0.205	0.117	-0.357	0.234
I_p (mm^4)	435	0.95	0.135	0.073	0.224	0.117	-0.112	0.234
I_{max} (mm^4)	434	0.64	0.1	0.057	0.219	0.117	-0.18	0.234
I_{min} (mm^4)	436	0.31	0.04	0.254	0.202	0.117	-0.089	0.233
Ct.Ar (mm^2)	435	1.45	0.13	0.197	0.218	0.117	-0.081	0.234
Ct.TMD ($g*mm^{-3}$)	435	980	18	0	-0.425	0.117	1.43	0.234

Distribution of Bone Indices and Properties from the Neck and Head Region

Within the neck region, all trabecular indices were normally distributed except BV and Tb.Sp (Shipiro-Wilk $p<0.05$) [Table 8]. BV was positively skewed and had a normal peak height; in contrast, Tb.Sp was negatively skewed and has a leptokurtic peak. In addition, the neck region displays the greatest mean for Tb.N and the lowest mean for

all cortical indices and properties except Ct.Th and Ct.TMD [Appendix 1 & Appendix 2]. Similarly the cortical indices and properties of the neck were almost entirely normally distributed with the exception of Ct.Th (negatively skewed and platkurtic) and Ct.TMD (negatively skewed with a normally height peak) [Table 9]. Within the head region, Conn.D and Tb.Sp were non-normally distributed. Conn.D was slightly positively skewed with a normal peak, and Tb.Sp was negatively skewed with a leptokurtic peak [Table 10]. The head region displays the greatest mean for Tb.TMD [Appendix 1].

Table 8. Mean, SD, Shapiro-Wilk significance, skewness and kurtosis values of trabecular bone in the neck region. BV and Tb.Sp were non-normally distributed as tested y the Shapiro-Wilk test.

Descriptive Statistics of Trabecular Bone in the Neck Region

	N	Mean	SD	Shapiro-Wilk	Skewness		Kurtosis	
	Statistic	Statistic	Statistic	Sig.	Statistic	Std. Error	Statistic	Std. Error
BV (mm^3)	242	0.01	0.005	0.004	0.321	0.156	-0.512	0.312
BV/TV (%)	244	16	6	0.59	-0.131	0.156	0.21	0.31
Conn.D (mm^{-3})	240	186	84.1	0.12	0.197	0.157	-0.471	0.313
SMI	236	1.1	0.76	0.84	0.096	0.158	-0.190	0.316
Tb.N (mm^{-1})	212	11	2.35	0.054	0.166	0.167	0.138	0.333
Tb.Th (µm)	230	44	7	0.54	0.007	0.16	0.113	0.32
Tb.Sp (mm)	243	0.1	0.03	0	-0.4761	0.156	1.2	0.311
Tb.TMD ($g*mm^{-3}$)	241	489	62	0.143	0.02	0.157	0.567	0.312

Table 9. Mean, SD, Shapiro-Wilk significance, skewness and kurtosis values of cortical bone in the neck region. Ct.Th and Ct.TMD were non-normally distributed as tested y the Shapiro-Wilk test.

Descriptive Statistics of Cortical Bone in the Neck Region

	N	Mean	SD	Shapiro-Wilk	Skewness		Kurtosis	
	Statistic	Statistic	Statistic	Sig.	Statistic	Std. Error	Statistic	Std. Error
Ct.BV (mm^3)	241	0.21	0.02	0.26	-0.123	0.157	0.437	0.312
Ct.BV/TV (%)	234	49	8.5	0.1	0.225	0.159	-0.099	0.317
Ct.Th (µm)	242	209	16	0.001	-0.368	0.156	-0.498	0.312
I_p (mm^4)	241	0.07404	0.013	0.07	0.095	0.157	0.253	0.312
I_{max} (mm^4)	236	0.047	0.008	0.15	0.268	0.158	-0.119	0.316
I_{min} (mm^4)	242	0.03	0.004	0.09	-0.017	0.156	-0.002	0.312
Ct.Ar (mm^2)	240	0.53	0.04	0.13	-0.193	0.157	0.365	0.313
Ct.TMD ($g*mm^{-3}$)	242	968	23	0.001	-0.54	0.156	0.556	0.312

Table 10. Mean, SD, Shapiro-Wilk significance, skewness and kurtosis values of trabecular bone in the head region. Conn.D and Tb.Sp were non-normally distributed as tested y the Shapiro-Wilk test.

Descriptive Statistics of Trabecular Bone in the Head Region

	N	Mean	SD	Shapiro-Wilk	Skewness		Kurtosis	
	Statistic	Statistic	Statistic	Sig.	Statistic	Std. Error	Statistic	Std. Error
BV (mm^3)	244	0.16	0.02	0.94	0.2	0.156	0.066	0.31
Conn.D	235	308	91	0.003	0.315	0.159	-0.295	0.316
SMI	236	1.1	0.8	0.76	0.096	0.158	-0.19	0.316
Tb.N (mm^{-1})	244	10	0.9	0.56	-0.159	0.156	-0.287	0.31
Tb.Th (µm)	241	84	10	0.183	0.267	0.157	-0.389	0.312
Tb.Sp (mm)	243	0.1	0.03	0	-0.476	0.156	1.202	0.311
Tb.TMD ($g*mm^{-3}$)	241	489	62	0.12	0.02	0.157	0.567	0.312

Correlations of Mouse Weight, Femora Length and Femoral Morphology

In order to test whether mouse weight and femora length is a factor in the degree of site specificity on the femur, correlations were made between all three variables. All non-normally distributed values were excluded from correlations analysis in this section and all other sections. In general, weight and length had very little correlation almost all of the indices and properties of trabecular and cortical bone. Of the existing significant correlations, the distal end (DE and DM) of the femur displayed the majority of them [Table 11]. Significant correlations within MD, PM, N and H were almost completely non-existent. There was no particular pattern that indicated an index was more favorable between any of the significant correlations. Similarly the significant correlations were so few that neither length nor weight could be assumed to be more correlated than the other.

Table 11. In bold are the display of existing correlations of trabecular and cortical bone with mouse weight and length. (A&B) Displays the few significant correlations in the DE region, (C) display those in the DM region and (D) displays those in the N region.

A. Correlations Between DE Trabecular Bone, Weight and Length

		BV	BV/TV	SMI	Tb.Th	Tb.Sp
Weight	Pearson Correlation	**-.18***	0.03	-0.06	-0.01	-0.12
	Sig. (2-tailed)	**0.033**	0.72	0.49	0.91	0.16
	N	141	138	141	141	141
Length	Pearson Correlation	0.07	-0.05	0.07	0.028	0.061
	Sig. (2-tailed)	0.22	0.40	0.26	0.63	0.3
	N	291	286	295	295	291

B. Correlations Between the DE Cortical Bone, Weight and Length

		Ct.BV	I_p	I_{max}	I_{min}	Ct.Ar	Ct.TMD
Weight	Pearson Correlation	**.238***	0.05	0.07	-0.001	**.238***	0.04
	Sig. (2-tailed)	**0.005**	0.57	0.41	0.99	**0.005**	0.66
	N	141	138	139	139	141	141
Length	Pearson Correlation	-0.02	0.067	0.051	0.054	-0.014	**.119***
	Sig. (2-tailed)	0.7	0.25	0.38	0.36	0.8	**0.04**
	N	293	291	292	292	292	641

C. Correlations Between DM Trabecular Bone, Weight and Length

		BV	BV/TV	Conn.D	SMI	Tb.N	Tb.TMD
Weight	Pearson Correlation	0.16	**.202***	0.04	**-.173***	0.03	**.214***
	Sig. (2-tailed)	0.05	**0.02**	0.66	**0.04**	0.69	**0.01**
	N	141	141	141	141	138	141
Length	Pearson Correlation	0.09	0.08	0.09	-0.07	**.128***	0.0900
	Sig. (2-tailed)	0.06	0.11	0.05	0.16	**0.01**	0.1000
	N	432	431	432	430	422	319

D. Correlations Between N Cortical Bone, Weight and Length

		N_Ct.BV	V	N_Ip	N_Imax	N_Imin	Ct.Ar	Ct.TMD
Weight	Pearson Correlation	-0.03	0.03	-0.08	-0.06	-0.09	-0.05	0.02
	Sig. (2-tailed)	0.73	0.71	0.36	0.48	0.29	0.56	0.8
	N	140	131	140	136	141	139	140
Length	Pearson Correlation	**-.168***	-0.05	-0.10	-0.12	-0.10	**-.161***	-0.022
	Sig. (2-tailed)	**0.009**	0.42	0.11	0.06	0.11	**0.013**	0.73
	N	241	234	241	236	242	240	242

Correlations of Trabecular Bone within the Regions of the Femur

In order to determine the number of site-specific regions within the femur, a correlation and linear regression analysis was performed for the six predefined ROIs. A correlation analysis indicates that depending on the microarchitectural index, there may be multiple independent morphological regions within an entire bone. In trabecular bone correlations, the distal epiphysis is independent of the other four trabecular regions when examining all morphological indices (except Tb.Th: Pearson correlation p value > 0.05).

Distal and proximal metaphyses are two regions that show the greatest number of moderate correlations among the different trabecular traits (R-squared = 23% - 46%, p value <0.05); the second greatest number of moderate correlations among all trabecular traits are between the distal metaphysis and head region [Table 12 and illustrated in Figure 9]. There were no correlations of Tb.TMD in any regions with normally distributed values. Thus, it can be concluded that none of the five femoral trabecular regions are significantly associated with one another across all trabecular indices.

Table 12. This chart displays statistically significant (p<0.05) correlations and regressions between trabecular regions (H, N, PM, DM, and DE) of the mouse (n=106) femora and morphological indices (BV, BV/TV, Conn.D, SMI, Tb.N, Tb.Th, and Tb.Sp). The italic bold numbers represent regression values.

Significant Correlations and Regressions of Trabecular Bone From Multiple Femoral Regions, p <0.05

		DM		N		H	
BV	PM	0.58	***0.34***				
	DM					0.57	***0.32***
BV/TV	PM	0.57	***0.32***				
	DM			0.33	***0.11***		
Conn.D	PM	0.44	***0.2***	0.22	***0.05***		
SMI	PM	0.49	***0.24***	0.34	***0.12***	0.34	***0.12***
	DM			0.3	***0.09***	0.3	***0.08***
Tb.N	DM			-0.34	***0.12***	0.57	***0.33***
Tb.Th	PM			0.36	***0.13***	0.38	***0.15***
	H			0.3	***0.01***		
Tb.Sp	PM	0.03	0.09				
Tb.TMD	DM			0.39	***0.15***	0.39	***0.15***
	N					1	***1***

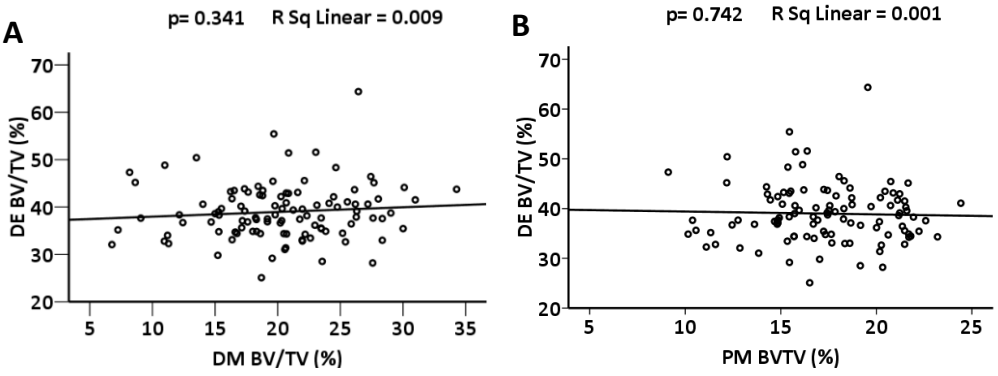

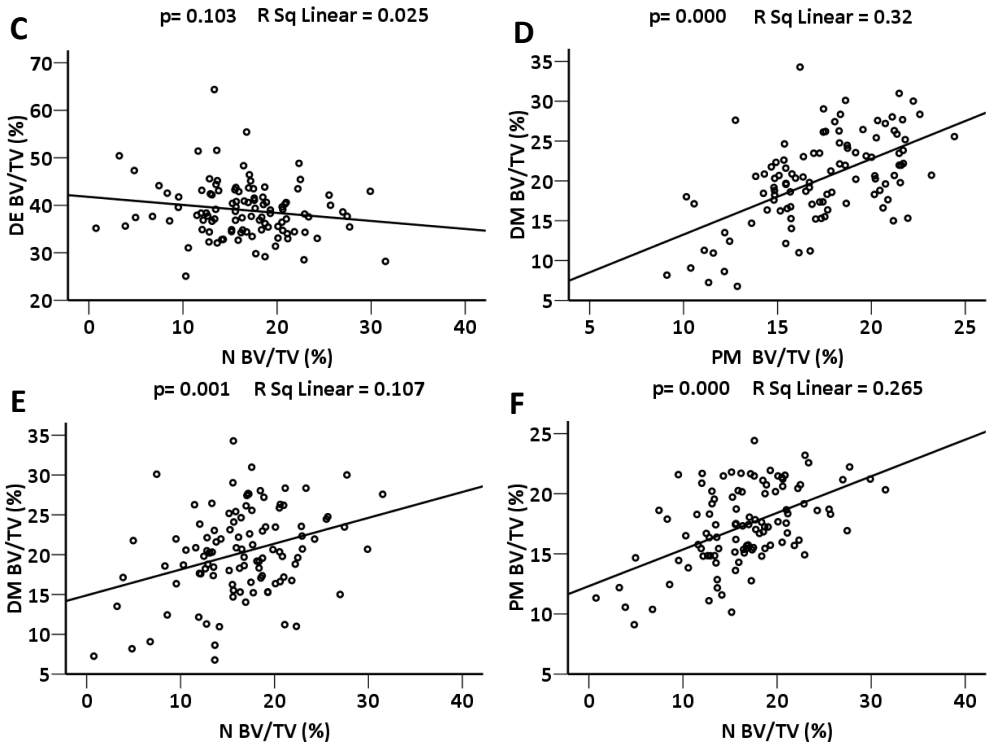

Figure 9. Linear regression analysis between the different trabecular regions of the femur (DE, DM, MD, PM, N). Each graph represents a regression of BV/TV (%) with a sample of 106 mice. Significant relationships exist between (D) DM vs PM, (E) DM vs N (weak), and (F) PM vs N.

Correlations of Cortical Bone within the Regions of the Femur

Unlike trabecular bone, cortical bone is a continuous region throughout the entire bone. Cortical regions were significantly correlated for nearly all morphological parameters. In addition, most of the relationships between the cortical indices of each region had moderate to strong correlations [Table 13 and Figure 10]. Properties that estimate resistance to torsional and bending rigidity exhibited the strongest correlations between the regions of the femur, especially when comparing the diaphysis and distal metaphysis, and the diaphysis and the proximal metaphysis. There were no correlations of Ct.TMD in any regions with normally distributed values.

Table 13. This chart displays statistically significant ($p<0.05$) correlations and regressions between cortical regions (N, PM, MD,DM, and DE) of the mouse (n=106) femora and morphological indices (Ct.BV, Ct.BV/TV, Ct.Th, I_p, I_{max}, I_{min}, and Ct.Ar). The italic bold numbers represent regression values.

Significant Correlations and Regressions of Cortical Bone From Multiple Femoral Regions, p <0.05

		DM		MD		PM		N	
Ct.BV	DE	0.42	***0.18***	0.44	***0.26***	0.43	***0.22***	0.34	***0.12***
	DM			0.66	***0.43***	0.52	***0.32***	0.34	***0.11***
	MD					0.51	***0.37***	0.59	***0.35***
	N							0.31	***0.17***
Ct.BV/TV	MD							0.20	***0.04***
Ct.Th	DM			0.38	***0.15***				
I_p	DE	0.54	***0.34***	0.66	***0.15***	0.56	***0.31***	0.46	***0.21***
	DM			0.84	***0.7***	0.75	***0.57***	0.51	***0.27***
	MD					0.75	***0.56***	0.65	***0.43***
	PM							0.47	***0.22***
I_{max}	DE	0.63	***0.39***	0.69	***0.47***	0.59	***0.34***	0.42	***0.17***
	DM			0.83	***0.69***	0.71	***0.5***	0.44	***0.2***
	MD					0.72	***0.52***	0.59	***0.35***
	PM							0.41	***0.17***
I_{min}	DE			0.57	***0.33***	0.51	***0.26***	0.52	***0.27***
	MD					0.76	***0.58***	0.71	***0.5***
	PM							0.56	***0.31***
Ct.Ar	DE	0.42	***0.18***	0.44	***0.2***	0.43	***0.22***	0.34	***0.12***
	DM			0.67	***0.43***	0.52	***0.328***	0.34	***0.11***
	MD					0.51	***0.37***	0.59	***0.35***
	PM							0.31	***0.17***

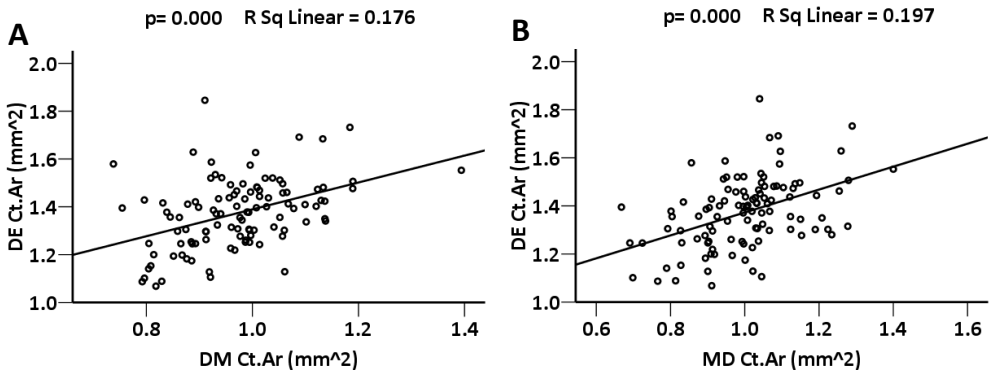

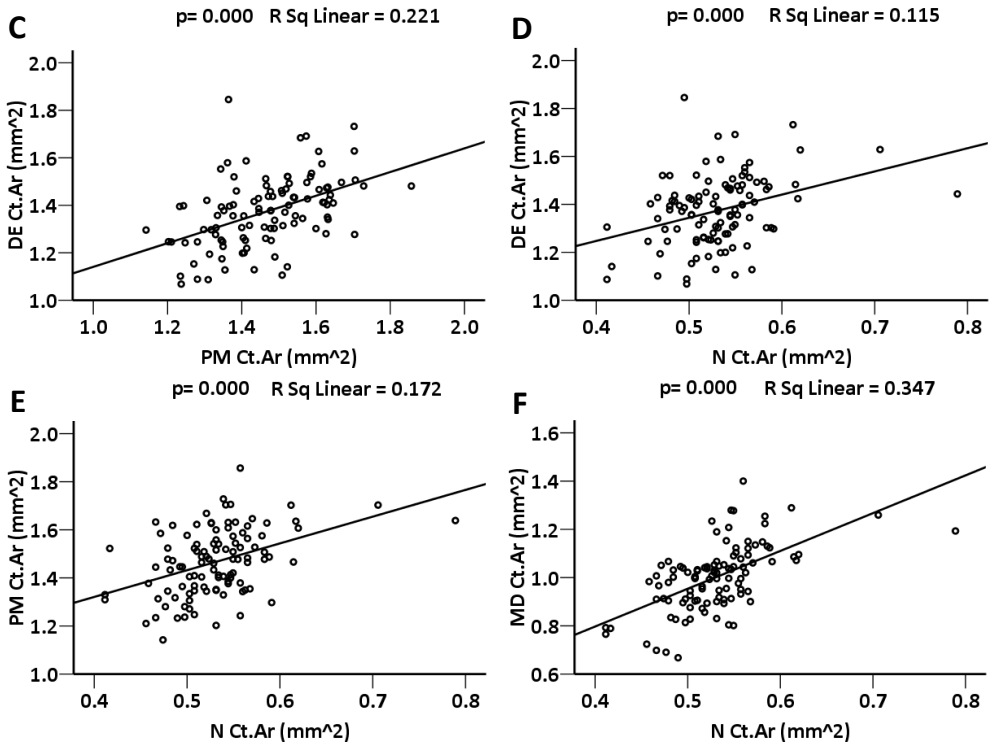

Figure 10. Linear regression analysis between the different cortical regions of the femur (DE, DM, MD, PM, N). Each graph represents a regression of BV/TV (%) with a sample of 106 mice. Significant relationships exist between all regions (A, B, C, D (weak), E, F).

Correlations of Trabecular and Cortical Bone

All femoral trabecular regions have a low to moderate correlation with femoral cortical bone, which suggests that inter-compartment regions are independent within an entire bone. When correlating trabecular bone to cortical bone, the degree of correlation varied when comparing it to correlations of just trabecular regions and of just cortical regions. The degree of correlation grew stronger when looking at the correlation groups in the following order: trabecular regions correlated to other trabecular regions; trabecular regions correlated to other cortical regions; and cortical regions correlated to other cortical regions. The degree of correlation between trabecular and cortical bone varies within the two regions. Trabecular bone of the head region shows the greatest degree of correlation with cortical bone [Table 14, A]. Conversely, the distal epiphysis has the least number of correlations among all trabecular regions and indices; and the strength of these correlations were weak [Table 14, B]. Figure 11 illustrates the results in the form of correlation graphs.

Table 14. Significant correlations and regressions between trabecular (BV, BV/TV, SMI, Tb.N, Tb.Th, and Tb.Sp) and cortical regions (Ct.Ar in (A); I_{min} in (B)). Bold Italics represent regressions values.

A. Significant Correlations and Regressions Between Cortical Ct.Ar and Trabecular Bone

	DE		DM		PM		N		H	
BV	0.28	***0.08***	0.57	***0.33***	0.58	***0.34***				
BV/TV			0.35	***0.12***	0.42	***0.18***	0.39	***0.15***		
SMI			0.36	***0.13***			0.29	***0.08***	0.29	***0.08***
Tb.N							0.31	***0.09***	0.3	***0.09***
Tb.Th	0.28	***0.08***			0.32	***0.1***	0.51	***0.26***		
Tb.Sp										

B. Significant Correlations and Regressions Between Cortical I_{min} and Trabecular Bone

	DE		PM		N		H	
BV	0.3	***0.09***	0.53	***0.29***				
BV/TV			0.31	***0.1***	0.35	***0.12***		
SMI					0.25	***0.06***	0.25	***0.06***
Tb.N					0.26	***0.07***		
Tb.Th	0.34	***0.12***	0.27	0.07	0.47	***0.22***		

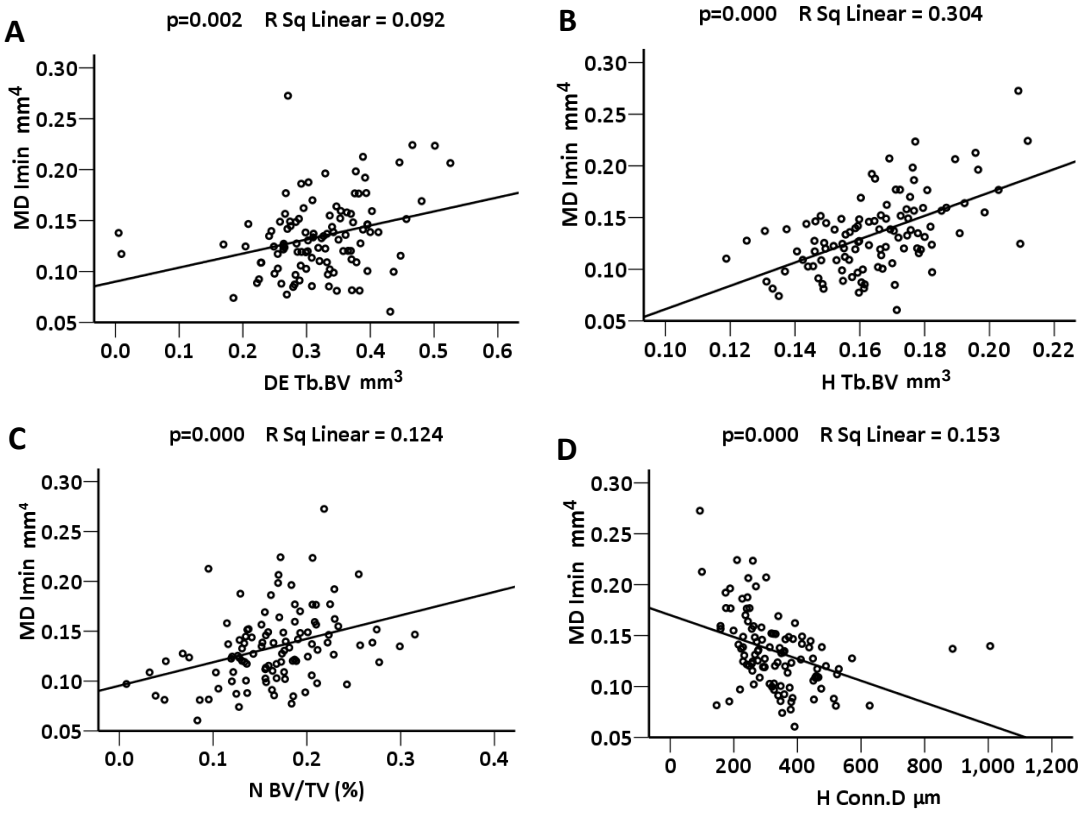

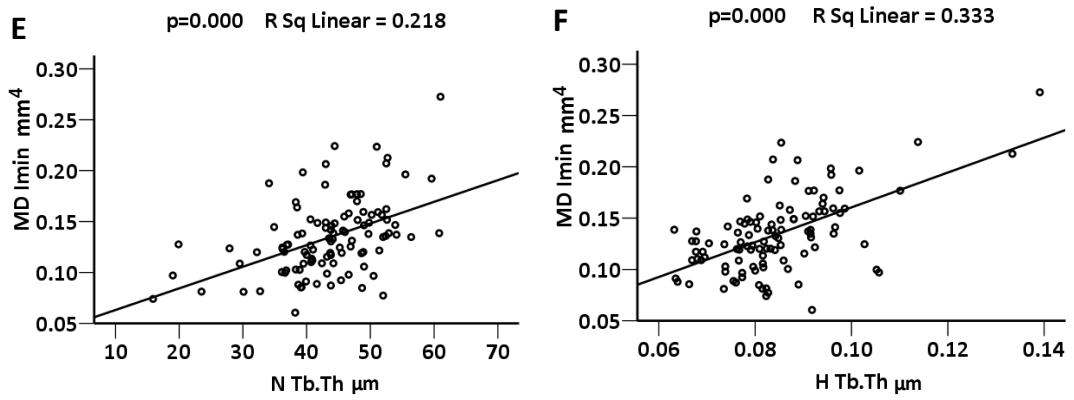

Figure 11. The correlation between trabecular bone and cortical bone varies depending on the region at which trabecular bone is being considered. Each graph displays significant correlations and regressions (A (weak), B, C (weak), D (weak), E,and F).

Trabecular and Cortical Correlations after Considering Weight and Length

Although not significantly correlated, we analyzed whether there existed an underlying influence of weight and length that cannot be seen through simple correlations. By removing the affect of weight and length during correlations it was found that mouse weight and femora length have little influence on the resulting correlation, as is illustrative in [Table 15]. Running partial correlations allowed us to test the influence of mouse weight and femora length as controlled variables. The correlation between PM and DM is 0.566 when considering the influence of the controlled variables, however, when removing these variables the value changes to 0.561. However, there is no pattern that indicates trabecular or cortical bone correlation values increase or decrease once controlled variables are removed. When the influence of these controlled variables was excluded from the correlations, there was a very small change in the correlation values. The change was so small that correlations that were moderate remained moderate and those that were high remained high. Similar results were seen when the comparison was taken over to cortical bone, as weight and length barely influenced correlations between cortical regions [Table 16]. The partial correlations showed very little influence from weight and length on the correlations between cortical bone regions. The correlation between PM and MD is 0.61 when considering the influence of the controlled variables, however, when the influence is removed the controlled variables the value changes to 0.614.

Table 15. Bivariate and Partial correlations were made between trabecular regions for BV/TV; the controlled variables were mouse weight and femora length. Results indicate that the controlled variables displayed little influence in the associations between trabecular regions.

Correlations of Bone Volume Fraction Between All Trabecular Regions of the Femur

Control Variables			DE	DM	PM	N	Weight	Length
none (Pearson)	DE	Correlation	1.000	.093	-.032	-.159	-.089	.071
		Significance (2-tailed)	.	.341	.742	.103	.366	.470
		df		104	104	104	104	104
	DM	Correlation		1.000	.566	.327	.110	.233
		Significance (2-tailed)		.	.000	.001	.262	.016
		df			104	104	104	104
	PM	Correlation			1.000	.515	.078	.084
		Significance (2-tailed)			.	.000	.427	.389
		df				104	104	104
	N	Correlation				1.000	-.038	.072
		Significance (2-tailed)				.	.696	.464
		df					104	104
	Weight	Correlation					1.000	.067
		Significance (2-tailed)					.	.430
		df						139
	Length	Correlation						1.000
		Significance (2-tailed)						.
		df						
Weight & Length	DE	Correlation	1.000	.089	-.032	-.170		
		Significance (2-tailed)	.	.368	.747	.084		
		df		102	102	102		
	DM	Correlation		1.000	.561	.326		
		Significance (2-tailed)		.	.000	.001		
		df			102	102		
	PM	Correlation			1.000	.517		
		Significance (2-tailed)			.	.000		
		df				102		
	N	Correlation				1.000		
		Significance (2-tailed)				.		
		df						

Table 16. Bivariate and Partial correlations were made between cortical regions for Ct.Ar; the controlled variables were mouse weight and femora length. Results indicate that the controlled variables displayed little influence in the associations between cortical regions.

Correlations of Cortical Area Between All Cortical Regions of the Femur

Control Variables			DE	DM	MD	PM	N	Weight	Length
none (Pearson)	DE	Correlation	1.000	.419	.444	.470	.339	.117	.041
		Significance (2-tailed)	.	.000	.000	.000	.000	.233	.680
		df		104	104	104	104	104	104
	DM	Correlation		1.000	.659	.563	.337	-.088	.255
		Significance (2-tailed)		.	.000	.000	.000	.371	.008
		df			104	104	104	104	104
	MD	Correlation			1.000	.610	.589	.069	.020
		Significance (2-tailed)			.	.000	.000	.485	.836
		df				104	104	104	104
	PM	Correlation				1.000	.414	-.037	.044
		Significance (2-tailed)				.	.000	.703	.656
		df					104	104	104
	N	Correlation					1.000	.135	.046
		Significance (2-tailed)					.	.168	.640
		df						104	104
	Weight	Correlation						1.000	.067
		Significance (2-tailed)						.	.430
		df							139
	Length	Correlation							1.000
		Significance (2-tailed)							.
		df							
Weight & Length	DE	Correlation	1.000	.441	.440	.477	.327		
		Significance (2-tailed)	.	.000	.000	.000	.001		
		df		102	102	102	102		
	DM	Correlation		1.000	.689	.571	.356		
		Significance (2-tailed)		.	.000	.000	.000		
		df			102	102	102		
	MD	Correlation			1.000	.614	.586		
		Significance (2-tailed)			.	.000	.000		
		df				102	102		
	PM	Correlation				1.000	.422		
		Significance (2-tailed)				.	.000		
		df					102		
	N	Correlation					1.000		
		Significance (2-tailed)					.		
		df							

Chapter 4

Discussion

Devices like high resolution μCT will be able to accurately predict fracture risk better than the current standards, yet proper accuracy also requires the understanding of the degree of specificity in which morphology is defined at different bones sites [30, 59, 60]. The goal of this study was to determine the overall degree of site specificity that exists in an entire bone for a heterogeneous population. We hypothesize that regional morphologies are not correlated in an entire bone for a heterogeneous population.

Mice were used in this study with the assumption that they prove as a proof of principle for the human skeleton. All values attained using the algorithm was well within the range of magnitudes reported in previous studies [46, 47, 58]. Some of the distributions of morphological traits in our mice population were found to be unpredictable as expected. In addition, the correlation results indicated that trabecular bone in general consisted of independent morphological sites as almost none were correlated with one another; and those that were correlated had weak correlations. The results also indicate that trabecular bone in distal epiphysis is completely independent from trabecular bone in other regions of the femur as it had no significant correlations for any trabecular index between any regions. The cortical regions of the entire femur were perhaps well correlated because of its mechanical properties. The polar moments of inertia for the cortical shell showed greater statistical significance than any of the other variables. No assumptions may be made on trabecular bone in regards to mechanical properties as they were not tested in this study. The moderate association between trabecular and cortical bone were mainly found at DM and PM, regions adjacent to MD. After testing the effects of weight and length on bone morphology and its properties, no significant influence can be seen by these to variables that may influence the degree of site-specificity. Each of these results will be further expounded upon in the paragraphs below.

In the second generation (F2) offspring, trabecular and cortical values from almost all regions did not differ significantly from normal distributions. The interesting relationship of our parental means and offspring distributions may perhaps be attributable to multiple interactions of many genes controlling the microarchitectural traits. Gene polymorphisms jointly influence bone mineral density loss in African-American women [61]. Considering that both parental strains have alleles that positively and negatively influence bone phenotype, the distribution in F2 offspring may be a result of independent assortments of the allele [62].

We correlated the defined regions by trabecular bone or cortical bone, and then by trabecular versus cortical bone using many different indices. Previous studies have shown that BMD alone provides a small amount of predictability for fracture risk [63]. In our study, TMD indicated correlations between trabecular regions and not cortical regions. However, this is an extrapolation as few TMD values could be used for

correlations since many of them were non- normally distributed. However, it is assumed that the parameters used to define bone site-specificity will be as insightful as BMD in predicting fracture risk. In addition, our results suggest that morphological regions may be associated with one another, but not necessarily because they are in proximity with one another. For example, in our study PM and DM were well correlated in trabecular regions despite trabecular bone not having many correlations in general. Even within the cortical correlations, there was no consistent indication that adjacent regions had greater correlated values than with non-adjacent regions. This, slightly contradicts a previous study that found greater proximity was indicative of greater associations [55]. It only slightly contradicts because our cortical results for polar moment of inertia indicate that adjacent correlations exist and are strongly significant. It is perhaps the case that the mechanical property of our cortical bone plays a role in maintaining great associations between adjacent regions. Although the mechanical properties for trabecular bone were not acquired for this study, the fact that they come from the individual struts (not the case in cortical bone) may be influencing trabecular independency.

The difference between trabecular bones versus cortical bone when comparing regional associations may be due to the different set of genes that control both compartments. Studies have shown that both compartments can be controlled by the same genes during the development of both compartments, mainly as a result of the requirement of cortical bone interacting with trabeculae during development [64]. These results suggest that while growing to adulthood, there is a change in gene expression such that site specificity may be imposed. Other regulatory mechanisms that may influence different regional associations between bone compartments also could be the result of genes controlling bone turnover. Studies demonstrate that bone turnover is controlled differently in the compartments, probably because of the different environments of bone cells from each compartment [65]. One particular study indicates that one such environment may be physiological and cellular, where overproduction of cathepsin K causes for resorption of both bone compartments and also the increase of thickness and mineral density of cortical bone [66]. This study suggests that trabecular bone turnover is likely influenced by local osteotropic cytokines where cortical bone is influenced by more systemic osteotropic hormones. This increase in cortical bone was also associated with the preservation of mechanical properties in the cortical shell. Thus, cellular, physiological and mechanical environments are all likely interconnected in affecting the difference of site-specificity between trabecular and cortical bone.

The moderate correlation between cortical and trabecular bone suggests that although trabecular sites are independent from one another, their relationship with cortical bone is not a site-specific one. Previous studies have shown that total body moss has a strong association with cortical bone mass (R-squared = 0.904, p-value =0.0001), but not as strong with trabecular bone mass (R-squared = 0.479, p-value =0.0001) [67]. This suggests that the relationship that exists between cortical and trabecular bone may perhaps be reflective of one that is independent in defining the site specific trabecular morphology and the systemic cortical morphology. Elucidating this relationship may provide more insight to the degree of trabecular site specificity in an entire bone.

In our study, we have shown that trabecular bone can be correlated with cortical bone within a bone but at a different site. In a similar study with adult females [52], genes

associated with BMP2 had stronger correlations with bone morphology peripherally than axially. Thus, in these correlations, trabecular bone seems less site-specific; however, this may be due to having a correlation between peripheral sites. In a sense, a correlation as more likely to exist at sites across the bones cross section than at sites along the length of the bone. It may perhaps be the case that local factors between cortical and trabecular are highlight in such peripheral correlations that may otherwise be hidden in an axial correlation.

Using mouse weight and bone length as factors to help predict site-specificity in bone morphology did not prove fruitful in our correlations. Body weight, however, has been found to be a factor in site-specific bone composition , where depending on the site bone composition changes with body weight [68]. In one particular study [69], an age-dependent change in trabecular morphology was found to significantly vary in degree depending on the bone site being observed. In addition, this relationship could only be seen in aged women and not men. If body weight and bone length could be coupled with age as factors in a study of site specificity in a female population, perhaps more would be elucidated to the amount of site-specific regions may exist in a bone. Perhaps coupling body weight and bone length with gender and age may elucidate an indirect relationship to the degree of site-specificity in the bone.

Clinically, it is imperative to define a method for identifying the weakest site (site most likely to fracture) in bone morphology. If the weakest site is either at a bone extremity or it can be interpreted from an extremity, scan exposure can be greatly reduced for patients while adequately assessing fracture risks. However, since there is site-specificity in trabecular bone and not in cortical bone, defining the weakest site only require the assessment of trabecular bone.

A limiting factor of the study was the difficulty in defining regions. In order to rigorously assess specificity, the number of predefined femoral regions could have been broken down even further. For example, instead of have one diaphyseal region, perhaps three could have been used and correlated among other broken down regions. It would of been interesting to see if site-specificity could be define between sites and their broken down versions. However, due to time limitations, such comparisons were not practical.

Conclusion

This study has shown that within a genetically heterogeneous population the femur exhibits site-specific morphology and was predominately in the trabecular bone. Thus future methods need to focus on how to reduce scanning exposure on cortical regions since any site on the bone is generally representative of other sites. In addition, scans for trabecular regions need to require more assessment since they vary site-specifically within a bone. Thus, when incorporating methods to reduce scan exposure and time trabecular specificity must be taken in consideration. In the future, it will be useful to improve the understanding of the differences found between cortical and trabecular bone as this may also prove useful in defining a bones weakest link.

Bibliography

[1] Seeman E. Bone quality: the material and structural basis of bone strength. Journal of Bone and Mineral Metabolism l2008;26: 1-8.
[2] Sommerfeldt DW, Rubin CT. Biology of bone and how it orchestrates the form and function of the skeleton. Eur Spine J l2001;10 Suppl 2: S86-95.
[3] Paul JP. Force Actions Transmitted by Joints in the Human Body. Proceedings of the Royal Society of London. Series B, Biological Sciences l1976;192: 163-172.
[4] Seeman E, Delmas PD. Bone quality--the material and structural basis of bone strength and fragility. N Engl J Med l2006;354: 2250-61.
[5] Roger MDZ, Anthony J, Findlay W, Mark K, Ego S. Femoral neck shape and the spatial distribution of its mineral mass varies with its size: Clinical and biomechanical implications. Bone l2005;37: 243-252.
[6] Bouxsein ML. Determinants of skeletal fragility. Best Pract Res Clin Rheumatol l2005;19: 897-911.
[7] Bain SD, Rubin CT. Metabolic modulation of disuse osteopenia: endocrine-dependent site specificity of bone remodeling. J Bone Miner Res l1990;5: 1069-75.
[8] Qin YX, Rubin CT, McLeod KJ. Nonlinear dependence of loading intensity and cycle number in the maintenance of bone mass and morphology. J Orthop Res l1998;16: 482-9.
[9] Enlow D. Principles of bone remodeling: An account of post-natal growth and remodeling processes in long bones and mandible: Thomas; 1963.
[10] Ruff CB, Hayes WC. Cross-sectional geometry of Pecos Pueblo femora and tibiae--a biomechanical investigation: II. Sex, age, side differences. Am J Phys Anthropol l1983;60: 383-400.
[11] Sumner DR, Morbeck ME, Lobick JJ. Apparent age-related bone loss among adult female Gombe chimpanzees. Am J Phys Anthropol l1989;79: 225-34.
[12] Rauch F, Glorieux FH. Osteogenesis imperfecta. Lancet l2004;363: 1377-85.
[13] C.A. Lee TAE. The Bone Organ System: Form and Function. Boston: Academic Press; 2001.
[14] Gray H. Anatomy of the Human Body. Philadelphia: Lea & Febiger; 1918.
[15] Donahue HJ, McLeod KJ, Rubin CT, Andersen J, Grine EA, Hertzberg EL, Brink PR. Cell-to-cell communication in osteoblastic networks: cell line-dependent hormonal regulation of gap junction function. J Bone Miner Res l1995;10: 881-9.
[16] Mosley JR. Osteoporosis and bone functional adaptation: mechanobiological regulation of bone architecture in growing and adult bone, a review. J Rehabil Res Dev l2000;37: 189-99.
[17] Albright J SH. Bone: structural organization and remodedling dynamics. In: Albright J, Brand R (eds) The scientific basis of orthopaedics 2nd edn l1987: 161-198.
[18] Klein-Nulend J, Nijweide PJ, Burger EH. Osteocyte and bone structure. Curr Osteoporos Rep l2003;1: 5-10.

[19] Noble BS. The osteocyte lineage. Arch Biochem Biophys l2008;473: 106-11.
[20] Organization WH. Prevention and Management of Osteoperosis; 2008.
[21] Kelsey JL. Osteoporosis: Prevalence and incidence. In "Osteoporosis,". Proceedings of the NIH Concensus Development Conference l1984: 25-28.
[22] L.Joseph Melton III CC. Magnitude and Impact of Osteoporosis and Fractures. In: Osteoporosis, Second Edition: Academic Press; 2001.
[23] III LJM. Epidemiology of fractures. In "Osteoporosis: Etiology, Diagnosis, and Management" (B.L. Riggs and L.J. Melton III, eds). New York: Raven Press; 1988.
[24] Chrischilles EA, Butler CD, Davis CS, Wallace RB. A model of lifetime osteoporosis impact. Arch Intern Med l1991;151: 2026-32.
[25] A. Praemer SF, and D.P. Rice. Musculoskeletal Conditions in the United States. American Academy of Orthopaedic Surgeons l1992.
[26] Cooper C, Campion G, Melton LJ, 3rd. Hip fractures in the elderly: a world-wide projection. Osteoporos Int l1992;2: 285-9.
[27] Friedman AW. Important determinants of bone strength: beyond bone mineral density. J Clin Rheumatol l2006;12: 70-7.
[28] Sarkar S, Mitlak BH, Wong M, Stock JL, Black DM, Harper KD. Relationships between bone mineral density and incident vertebral fracture risk with raloxifene therapy. J Bone Miner Res l2002;17: 1-10.
[29] Watts NB, Cooper C, Lindsay R, Eastell R, Manhart MD, Barton IP, van Staa TP, Adachi JD. Relationship between changes in bone mineral density and vertebral fracture risk associated with risedronate: greater increases in bone mineral density do not relate to greater decreases in fracture risk. J Clin Densitom l2004;7: 255-61.
[30] Mittra E, Rubin C, Gruber B, Qin Y-X. Evaluation of trabecular mechanical and microstructural properties in human calcaneal bone of advanced age using mechanical testing, [mu]CT, and DXA. Journal of Biomechanics l2008;41: 368-375.
[31] Nguyen TV, Eisman JA. Genetics of fracture: challenges and opportunities. J Bone Miner Res l2000;15: 1253-6.
[32] Smith DM, Nance WE, Kang KW, Christian JC, Johnston CC, Jr. Genetic factors in determining bone mass. J Clin Invest l1973;52: 2800-8.
[33] Eisman JA. Genetics of Osteoporosis. Endocr Rev l1999;20: 788-804.
[34] Ferrari S, Rizzoli R, Bonjour JP. Genetic aspects of osteoporosis. Curr Opin Rheumatol l1999;11: 294-300.
[35] Deng HW, Chen WM, Recker S, Stegman MR, Li JL, Davies KM, Zhou Y, Deng H, Heaney R, Recker RR. Genetic determination of Colles' fracture and differential bone mass in women with and without Colles' fracture. J Bone Miner Res l2000;15: 1243-52.
[36] Andrew T, Antioniades L, Scurrah KJ, Macgregor AJ, Spector TD. Risk of wrist fracture in women is heritable and is influenced by genes that are largely independent of those influencing BMD. J Bone Miner Res l2005;20: 67-74.
[37] Arden NK, Baker J, Hogg C, Baan K, Spector TD. The heritability of bone mineral density, ultrasound of the calcaneus and hip axis length: a study of postmenopausal twins. J Bone Miner Res l1996;11: 530-4.
[38] Garnero P, Arden NK, Griffiths G, Delmas PD, Spector TD. Genetic influence on bone turnover in postmenopausal twins. J Clin Endocrinol Metab l1996;81: 140-6.

[39] Andre D Uitterlinden JPTMVL, and Huibert A.P. Pols. Genetics and Genomics of Osteoporosis. In: Robert Marcus DF, Jennifer Kelsey, editor. Osteoporosis, Second Edition. San Diego: Academic Press; 2001.
[40] Einhorn TA. Bone strength: the bottom line. Calcif Tissue Int l1992;51: 333-9.
[41] Guo XE, Kim CH. Mechanical consequence of trabecular bone loss and its treatment: a three-dimensional model simulation. Bone l2002;30: 404-11.
[42] Legrand E, Chappard D, Pascaretti C, Duquenne M, Krebs S, Rohmer V, Basle MF, Audran M. Trabecular bone microarchitecture, bone mineral density, and vertebral fractures in male osteoporosis. J Bone Miner Res l2000;15: 13-9.
[43] Cummings SR, Nevitt MC, Browner WS, Stone K, Fox KM, Ensrud KE, Cauley J, Black D, Vogt TM. Risk factors for hip fracture in white women. Study of Osteoporotic Fractures Research Group. N Engl J Med l1995;332: 767-73.
[44] El-Kaissi S, Pasco JA, Henry MJ, Panahi S, Nicholson JG, Nicholson GC, Kotowicz MA. Femoral neck geometry and hip fracture risk: the Geelong osteoporosis study. Osteoporos Int l2005;16: 1299-303.
[45] Ammann P, Rizzoli R, Meyer JM, Bonjour JP. Bone density and shape as determinants of bone strength in IGF-I and/or pamidronate-treated ovariectomized rats. Osteoporos Int l1996;6: 219-27.
[46] Judex S, Garman R, Squire M, Donahue LR, Rubin C. Genetically based influences on the site-specific regulation of trabecular and cortical bone morphology. J Bone Miner Res l2004;19: 600-6.
[47] Judex S, Garman R, Squire M, Busa B, Donahue LR, Rubin C. Genetically linked site-specificity of disuse osteoporosis. J Bone Miner Res l2004;19: 607-13.
[48] Ward WE, Kim S, Chan D, Fonseca D. Serum equol, bone mineral density and biomechanical bone strength differ among four mouse strains. J Nutr Biochem l2005;16: 743-9.
[49] Fonseca D, Ward WE. Daidzein together with high calcium preserve bone mass and biomechanical strength at multiple sites in ovariectomized mice. Bone l2004;35: 489-97.
[50] Choi JY, Shin CS, Hong YC, Kang D. Single-nucleotide polymorphisms and haplotypes of bone morphogenetic protein genes and peripheral bone mineral density in young Korean men and women. Calcif Tissue Int l2006;78: 203-11.
[51] Zhang H, Sol-Church K, Rydbeck H, Stabley D, Spotila LD, Devoto M. High resolution linkage and linkage disequilibrium analyses of chromosome 1p36 SNPs identify new positional candidate genes for low bone mineral density. Osteoporos Int l2008.
[52] McGuigan FE, Larzenius E, Callreus M, Gerdhem P, Luthman H, Akesson K. Variation in the BMP2 gene: bone mineral density and ultrasound in young adult and elderly women. Calcif Tissue Int l2007;81: 254-62.
[53] Fritton JC, Myers ER, Wright TM, van der Meulen MC. Loading induces site-specific increases in mineral content assessed by microcomputed tomography of the mouse tibia. Bone l2005;36: 1030-8.
[54] Ng AH, Wang SX, Turner CH, Beamer WG, Grynpas MD. Bone quality and bone strength in BXH recombinant inbred mice. Calcif Tissue Int l2007;81: 215-23.

[55] Sabsovich I, Clark JD, Liao G, Peltz G, Lindsey DP, Jacobs CR, Yao W, Guo TZ, Kingery WS. Bone microstructure and its associated genetic variability in 12 inbred mouse strains: microCT study and in silico genome scan. Bone l2008;42: 439-51.
[56] Shultz KL, Donahue LR, Bouxsein ML, Baylink DJ, Rosen CJ, Beamer WG. Congenic strains of mice for verification and genetic decomposition of quantitative trait loci for femoral bone mineral density. J Bone Miner Res l2003;18: 175-85.
[57] Lublinsky S, Ozcivici E, Judex S. An automated algorithm to detect the trabecular-cortical bone interface in micro-computed tomographic images. Calcif Tissue Int l2007;81: 285-93.
[58] Squire M, Donahue LR, Rubin C, Judex S. Genetic variations that regulate bone morphology in the male mouse skeleton do not define its susceptibility to mechanical unloading. Bone l2004;35: 1353-60.
[59] Firoozabadi R, Morshed S, Engelke K, Prevrhal S, Fierlinger A, Miclau T, 3rd, Genant HK. Qualitative and quantitative assessment of bone fragility and fracture healing using conventional radiography and advanced imaging technologies--focus on wrist fracture. J Orthop Trauma l2008;22: S83-90.
[60] Muller M, Mitton D, Talmant M, Johnson P, Laugier P. Nonlinear ultrasound can detect accumulated damage in human bone. J Biomech l2008;41: 1062-8.
[61] Zmuda JM, Cauley JA, Danielson ME, Ferrell RE. Preliminary report: Vitamin D receptor and aromatase gene interaction and bone mass in older African-American women. Metabolism l2003;52: 521-523.
[62] Rosen CJ, Beamer WG, Donahue LR. Defining the genetics of osteoporosis: using the mouse to understand man. Osteoporos Int l2001;12: 803-10.
[63] Ruppel Me Fau - Miller LM, Miller Lm Fau - Burr DB, Burr DB. The effect of the microscopic and nanoscale structure on bone fragility.
[64] Tanck E, Hannink G, Ruimerman R, Buma P, Burger EH, Huiskes R. Cortical bone development under the growth plate is regulated by mechanical load transfer. J Anat l2006;208: 73-9.
[65] Mundy GR CD, Babatunde OO. Bone remodeling. In: Favus MJ, ed. Primer on the Metabolic Bone Diseases and Disorders of Mineral Metabolism 5ed. Philadelphia: Lippincott Williams & Wilkins; 2003.
[66] Morko J, Kiviranta R, Hurme S, Rantakokko J, Vuorio E. Differential turnover of cortical and trabecular bone in transgenic mice overexpressing cathepsin K. Bone l2005;36: 854-65.
[67] Rico H, Gonzalez-Riola J, Revilla M, Villa LF, Gomez-Castresana F, Escribano J. Cortical versus trabecular bone mass: influence of activity on both bone components. Calcif Tissue Int l1994;54: 470-2.
[68] Milliken LA, Cussler E, Zeller RA, Choi JE, Metcalfe L, Going SB, Lohman TG. Changes in soft tissue composition are the primary predictors of 4-year bone mineral density changes in postmenopausal women. Osteoporos Int l2008.
[69] Lochmuller EM, Matsuura M, Bauer J, Hitzl W, Link TM, Muller R, Eckstein F. Site-specific deterioration of trabecular bone architecture in men and women with advancing age. J Bone Miner Res l2008;23: 1964-73.

Appendix

Appendix 1. Descriptive statistics of trabecular bone in all regions in the heterogeneous, BALB and C3H population.

Trabecular Descriptive Statistics

		H		N		PM		DM		DE	
Population Type		Mean	SD	Mean	SD	Mean	SD	Mean	SD	Mean	SD
Heterogeneous Population	BV (mm^3)	0.16	0.02	0.01	0.005	0.15	0.03	0.52	0.15	0.33	0.06
	BV/TV (%)			16	6	17	3.3	20	5	39	4.6
	Conn.D (mm^{-3})	308	91	186	84.1	98	23	154	48	137	32
	SMI	1.1	0.8	1.1	0.76	0.64	0.36	1.4	0.42	-0.37	0.42
	Tb.N (mm^{-1})	10	0.9	11	2.35	5.1	0.43	4.9	0.66	6.5	0.43
	Tb.Th (µm)	84	10	44	7	59	4.5	55	5.5	72	6.9
	Tb.Sp (mm)	0.100	0.03	0.1	0.03	0.21	0.02	0.2	0.03	0.15	0.02
	Tb.TMD ($g*mm^{-3}$)	489	62	489	62	207	37	236	52	398	50
BALB	BV/TV (%)							9.7	2	29.5	2.3
	Conn.D (mm^{-3})							144	43	2.3	36
	Tb.Th (µm)							35.6	2.3	49.1	2.8
	Tb.N (mm^{-1})							4.8	0.3	7.1	0.4
	Tb.Sp (mm)							0.21	0.01	0.14	0.01
C3H	BV/TV (%)							16.2	3	29.5	2.4
	Conn.D (mm^{-3})							101	26	92	17
	Tb.Th (µm)							54.8	2.4	67.5	2.6
	Tb.N (mm^{-1})							4.4	0.4	6	0.4
	Tb.Sp (mm)							0.22	0.02	0.17	0.01

Appendix 2. Descriptive statistics of cortical bone in all regions in the heterogeneous, BALB and C3H population.

Cortical Descriptive Statistics

		N		PM		MD		DM		DE	
Population Type		Mean	SD	Mean	SD	Mean	SD	Mean	SD	Mean	SD
Heterogeneous Population	Ct.BV (mm^3)	0.21	0.02	0.66	0.059	0.76	0.09	1.4	0.14	0.48	0.048
	Ct.BV/TV (%)	49	8.5	89	3	99	0.1	79	3	75	6.5
	Ct.Th (μm)	209	16	213	16.7	312	33	156	14	109	14
	I_p (mm^4)	0.07	0.013	0.95	0.135	0.42	0.09	0.7	0.13	1.03	0.17
	I_{max} (mm^4)	0.05	0.008	0.64	0.1	0.29	0.07	0.49	0.09	0.57	0.09
	I_{min} (mm^4)	0.03	0.004	0.31	0.04	0.13	0.027	0.21	0.04	0.46	0.09
	Ct.Ar (mm^2)	0.530	0.04	1.45	0.13	0.56	0.12	0.96	0.1	1.3	0.13
	Ct.TMD ($g*mm^{-3}$)	968	23	980	18	1208	23	873	31	741	35
BALB	I_p (mm4)					0.43	0.05	0.77	0.07		
	I_{max} (mm^4)					0.32	0.04	0.54	0.04		
	I_{min} (mm^4)					0.12	0.01	0.22	0.03		
	Ct.Ar (mm^2)					0.95	0.05	0.84	0.04		
C3H	I_p (mm4)					0.61	0.06	0.98	0.11		
	I_{max} (mm^4)					0.43	0.05	0.62	0.14		
	I_{min} (mm^4)					0.18	0.02	0.35	0.14		
	Ct.Ar (mm^2)					1.3	0.09	1.12	0.06		

Appendix 3. Trabecular Correlations with regions in the femur. *Significant correlation $p<0.05$.

Correlations of BV in the Femur

		DE	DM	PM	H
DE	Pearson Correlation	1	0.052	0.125	0.184
	Sig. (2-tailed)		0.595	0.2	0.06
	N		106	106	106
DM	Pearson Correlation		1	.581*	.569*
	Sig. (2-tailed)			0	0
	N			106	106
PM	Pearson Correlation			1	.478*
	Sig. (2-tailed)				0
	N				106

Correlations of BV/TV in the Femur

		DE	DM	PM	N
DE	Pearson Correlation	1	0.093	-0.032	-0.159
	Sig. (2-tailed)		0.341	0.742	0.103
	N		106	106	106
DM	Pearson Correlation		1	.566*	.327*
	Sig. (2-tailed)			0	0
	N			106	106
PM	Pearson Correlation			1	.515*
	Sig. (2-tailed)				0
	N				106

Correlations of Conn.D in the Femur

		DM	PM	N
DM	Pearson Correlation	1	.443*	0.154
	Sig. (2-tailed)		0	0.114
	N		106	106
PM	Pearson Correlation		1	.219*
	Sig. (2-tailed)			0.02
	N			106

Correlations of SMI in the Femur

		DE	DM	PM	N	H
DE	Pearson Correlation	1	-0.0601	-0.0378	-0.0423	-0.0423
	Sig. (2-tailed)		0.54	0.7	0.667	0.667
	N		106	106	106	106
DM	Pearson Correlation		1	.489*	.295*	.295*
	Sig. (2-tailed)			0	0.002	0.002
	N			106	106	106
PM	Pearson Correlation			1	.340*	.340*
	Sig. (2-tailed)				0.00036	0.00036
	N				106	106
N	Pearson Correlation				1	1*
	Sig. (2-tailed)					0
	N					106

Correlations of Tb.N in the Femur

		DM	N	H
DM	Pearson Correlation	1	-.339*	.572*
	Sig. (2-tailed)		0.00038	0
	N		106	106
N	Pearson Correlation		1	-0.1651
	Sig. (2-tailed)			0.09
	N			106

Correlations of Tb.Th in the Femur

		DE	PM	N	H
DE	Pearson Correlation	1	-0.0586	0.003	.277*
	Sig. (2-tailed)		0.551	0.973	0.00404
	N		106	106	106
PM	Pearson Correlation		1	.357*	.382*
	Sig. (2-tailed)			0.00017	0
	N			106	106
N	Pearson Correlation			1	.299*
	Sig. (2-tailed)				0.002
	N				106

Correlations of Tb.Sp in the Femur

		PM
DE	Pearson Correlation	0.036
	Sig. (2-tailed)	0.71
	N	106

Correlations of Tb.TMD in the Femur

		DM	N	H
DM	Pearson Correlation	1	.389*	.389*
	Sig. (2-tailed)		0	0
	N		106	106
N	Pearson Correlation		1	1*
	Sig. (2-tailed)			0
	N			106

Appendix 4. Cortical Correlations with regions in the femur. *Significant correlation $p<0.05$.

Correlations of Ct.BV in the Femur

		DE	DM	MD	PM	N
DE	Pearson Correlation	1	.419*	.444*	.470*	.339*
	Sig. (2-tailed)		0	0	0	0.00039
	N		106	106	106	106
DM	Pearson Correlation		1	.659*	.563*	.337*
	Sig. (2-tailed)			0	0	0.00042
	N			106	106	106
MD	Pearson Correlation			1	.610*	.589*
	Sig. (2-tailed)				0	0
	N				106	106
PM	Pearson Correlation				1	.414*
	Sig. (2-tailed)					0
	N					106

Correlations Ct.Th in the Femur

		MD
DM	Pearson Correlation	.381*
	Sig. (2-tailed)	0
	N	106

Correlations of I_p in the Femur

		DE	DM	MD	PM	N
DE	Pearson Correlation	1.000	.583*	.655*	.560*	.460*
	Sig. (2-tailed)		0	0	0	0
	N		106	106	106	106
DM	Pearson Correlation		1	.836*	.753*	.514*
	Sig. (2-tailed)			0	0	0
	N			106	106	106
MD	Pearson Correlation			1	.749*	.652*
	Sig. (2-tailed)				0	0
	N				106	106
PM	Pearson Correlation				1	.472*
	Sig. (2-tailed)					0
	N					106

Correlations of I_{max} in the Femur

		DE	DM	MD	PM	N
DE	Pearson Correlation	1	.628*	.687*	.585*	.417*
	Sig. (2-tailed)		0	0	0	0
	N		106	106	106	106
DM	Pearson Correlation		1	.831*	.707*	.442*
	Sig. (2-tailed)			0	0	0
	N			106	106	106
MD	Pearson Correlation			1	.718*	.588*
	Sig. (2-tailed)				0	0
	N				106	106
PM	Pearson Correlation				1	.411*
	Sig. (2-tailed)					0
	N					106

Correlations of I_{min} in the Femur

		DE	MD	PM	N
DE	Pearson Correlation	1	.577*	.511*	.518*
	Sig. (2-tailed)		0	0	0
	N		106	106	106
MD	Pearson Correlation		1	.758*	.706*
	Sig. (2-tailed)			0	0
	N			106	106
PM	Pearson Correlation			1	.560*
	Sig. (2-tailed)				0
	N				106

Correlations of Ct.Ar in the Femur

		DE	DM	MD	PM	N
DE	Pearson Correlation	1	.419*	.444*	.470*	.339*
	Sig. (2-tailed)		0	0	0	0.00039
	N		106	106	106	106
DM	Pearson Correlation		1	.659*	.563*	.337*
	Sig. (2-tailed)			0	0	0.00042
	N			106	106	106
MD	Pearson Correlation			1	.610*	.589*
	Sig. (2-tailed)				0	0
	N				106	106
PM	Pearson Correlation				1	.414*
	Sig. (2-tailed)					0
	N					106

Correlations of Ct.TMD in the Femur

		DM
DE	Pearson Correlation	0.17
	Sig. (2-tailed)	0.09
	N	106